Preparation and characterisation of fillers for polymer nanocomposite layers usable in electronics

Thaiskang Jamatia, M.Sc., Ph.D.

Doctoral Thesis Summary

Tomas Bata University in Zlín

Tomas Bata University in Zlín
Faculty of Technology

Doctoral thesis summary

Preparation and characterisation of fillers for polymer nanocomposite layers usable in electronics

Příprava a charakterizace plniv pro polymerní nanokompozitní vrstvy využitelné v elektronice

Author: Thaiskang Jamatia, M.Sc., Ph.D.

Degree programme: P 2808 Chemistry and Materials Technology

Degree course: 2808V006 Technology of Macromolecular Compounds

Supervisor: Assoc. Prof. Ing. et Ing. Ivo Kuřitka, Ph.D. et Ph.D.

Consultants: Mgr. David Škoda, Ph.D.
                       Assoc. Prof. Ing. Jarmila Vilčáková, Ph.D.

External examiners: Asst. Prof. Ing. Radka Bálková, Ph.D.
                       doc. Dr. Ing. Vladimír Pavlínek, Ph.D.
                       prof. Ing. Petr Slobodian, Ph.D.

Zlín, September 2020

ACKNOWLEDGEMENT

CONTENT

ABSTRACT

The work centres on the one-pot microwave-assisted polyol synthesis of undoped and Fe- and Al-doped ZnO nanoparticles from zinc acetate precursor diethylene glycol (DEG) solution in 15 minutes. The microwave reactor is advantageous over conventional heating due to its rapid and uniform heating of the reaction mixtures. The main advantage of the polyol synthesis is its ability to reduce metal ions and passivation of surface defects in ZnO nanoparticles. The roles of small stoichiometric amounts of water and oleic acid (OA) as a capping agent in the synthesis were studied. The average particle size of undoped ZnO nanoparticles increases with the addition of multiples of equivalent amounts of water to the precursor solution. Also, the addition of the long-chain organic ligand, OA, yielded well-dispersed products without agglomerations. Moreover, it allowed fine dispersion of ZnO and doped ZnO nanoparticles in toluene which is necessary for the preparation of nanocomposites.

Doping of the ZnO nanoparticles was carried out for altering the band gap of the semiconductor nanoparticles to modify its optical and electronic properties. Fe^{3+} source ions were reduced to Fe^{2+}, and incorporated to the host crystal lattice of nanoparticles. This p-doping decreased the UV luminescence intensity of the host nanoparticles. Addition of Al^{3+} source to the reaction mixture resulted in n-doping of the host nanoparticles imparting them enhanced UV luminescent intensity.

The particle crystallinity and size of the nanocrystallites were analysed by X-ray diffraction (XRD), and transmission electron microscopy (TEM) images confirmed the morphology and size of the nanoparticles produced. Ultraviolet-visible spectroscopy (UV-Vis) and fluorescence measurement were conducted to analyse the optical properties of the nanoparticles. Diffuse reflectance (DR) UV-Vis measured the reflectance, and the band gap was estimated by Tauc plot. Brus' model was utilised to study the relation between the size of the semiconductor nanoparticles and its electronic structure.

Finally, polymer light-emitting diodes (PLEDs) were chosen to demonstrate the ability of the tailored nanoparticles as fillers for polymer-matrix nanocomposite-based electronic devices. The dispersions of pure or variously doped ZnO nanoparticles in toluene solutions of poly[2-methoxy-5-(2'-ethylhexyloxy)-1,4-phenylene vinylene] (MEH-PPV) were spin-cast to obtain thin nanocomposite films serving as emissive layers in PLEDs. Electroluminescence (EL) was increased by the introduction of the nanoparticles. Specifically, Fe-doping decreased the opening bias while Al-doping enhanced the EL greatly. Moreover, the chromaticity characteristics were improved by nanoparticles addition as well.

Keywords: microwave, polyol, zinc oxide, doping, nanoparticles, MEH-PPV, nanocomposites, polymer light-emitting diode.

3

ABSTRAKT

Práce se soustředí na jednokrokovou mikrovlnami asistovanou polyolovou syntézu nedopovaných a Fe- a Al-dopovaných nanočástic ZnO z octanu zinečnatého jako prekurzoru rozpuštěného v diethylen glykolu, která trvá vždy jen 15 minut. Mikrovlnný reaktor je výhodnější než konveční, díky rychlosti a uniformitě ohřevu reakční směsi. Hlavní výhodou polyolové syntézy je schopnost redukovat ionty kovů a pasivace defektů na povrchu ZnO nanočástic. Byla studována role malých stechiometrických množství vody, a také kyseliny olejové (OA) jako povrch modifikujícího činidla, při syntéze. Průměrná velikost částic nedopovaného ZnO vzrůstá s přídavkem násobků molárně ekvivalentních množství vody do roztoku prekurzoru. Přídavek organického ligandu s dlouhým řetězcem, OA, vedl ke vzniku dobře dispergovaného produktu bez aglomerátů, navíc to umožňuje připravit disperze nanočástic ZnO (dopovaných i nedopovaných) v toluenu, což je nutné pro přípravu nanokompozitů.

Dopování ZnO nanočástic bylo prováděno kvůli modifikaci zakázaného pásu polovodičových nanočástic pro úpravu jejich optických a elektronických vlastností. Fe^{3+} iony ze zdrojové soli se redukovaly na Fe^{2+} a byly přijaty do hostitelské krystalové mřížky nanočástic. Toto p-dopování potlačilo intenzitu UV luminiscence nanočástic. Přídavek zdroje Al^{3+} do reakční směsi vedl k n-dopování hostitelských nanočástic a nárůstu intenzity jejich UV luminiscence.

Krystalinita a velikost nanokrystalitů byly analyzovány rentgenovou difraktometrií (XRD) a transmisní elektronová mikroskopie (TEM) ověřila morfologii a velikost připravených nanočástic. Optické vlastnosti nanočástic byly analyzovány spektrometrií v ultrafialové a viditelné oblasti (UV-Vis) a měřeními fluorescence. Difuzně reflektanční (DR) UV-Vis měření reflektance umožnilo stanovení šířky zakázaného pásu z Taucova grafu. Brusova rovnice byla využita jako model pro studium vztahu velikosti nanočástice a jejich elektronické struktury.

Naposledy byly vybrány polymerní světlo emitující diody (PLED) jako příkladné elektronické prvky, aby se na nich demonstrovaly účinky tailorovaných nanočástic jako plniv pro nanokompozity s polymerní matricí pro využití v elektronice. Disperze čistých nebo různě dopovaných ZnO nanočástic v toluenových roztocích poly[2-methoxy-5-(2'-ethylhexyloxy)-1,4-fenylene vinylene] (MEH-PPV) byly nanášeny rotačním litím tak, aby se připravila tenká nanokompozitní vrstva sloužící po dohotovení přípravku jako samotná emisní vrstva v PLED. Intenzita elektroluminiscence se přidáním nanočástic do aktivní vrstvy zvyšovala. Přídavek Fe-dopovaných nanočástic snížil otevírací napětí diod, zatímco přídavek Al-dopovaných nanočástic zvýšil intenzitu EL. Navíc byly přídavkem nanočástic vylepšeny chromatické charakteristiky diod.

Klíčová slova: mikrovlny, polyol, oxid zienčnatý, dopování, nanočástice, MEH-PPV, nanokompozit, polymerní světlo emitující dioda.

1. INTRODUCTION

1.1 Research motivation

Nanoscience is the study of matter at the nanometre range (1 nm = 10^{-9} m). The scale of nanometre ranges from 1 to 100 nm. At this length, a material tends to have physical and chemical characteristics related to its size. Moreover, the classical Newtonian mechanics is not applicable; instead, it is the quantum mechanical system, which is at play here. It was in 1971 the term nanotechnology was coined by Norio Taniguchi. However, the idea was conceptualised in 1959 by Richard Feynman at an American Physical Society meeting in Caltech. One of the main reasons why the study of matter at the molecular and atomic level is important is due to its high surface-to-volume ratio. This phenomenon should not be surprising when materials at nanometre range display chemical and physical properties different from the bulk materials. It is due to the relatively larger surface area to the volume that the surface of a nanoparticle is more exposed, resulting in its high chemical reactivity.

Nanoscience and nanotechnology are found in various fields of science and technology due to its cutting-edge applications in medicines [1], gas sensing [2], agriculture [3], food packaging [4] etc. In the past few decades, there has been an increasing number of ongoing research of the semiconductor nanoparticles. As stated earlier, in the nanometre range (1-100 nm), materials behave differently from the bulk. The same nanomaterial exhibit different properties based on the size and shape of the nanomaterials; it is due to this fact, there are numerous researches in the field of semiconductor nanomaterials in both academia and industries. The semiconductor nanocrystals exhibit size-dependent properties. When the dimension of bulk material is reduced to nanometre range (1-100 nm), quantum confinement is achieved. As a result, the density of the electronic states becomes discrete at the edges of the band structure, resulting in the alteration of the electrical and optical properties of the bulk material [5].

In order to tap or harness these potentials of nanomaterials, researchers have continuously worked on the control and manipulation of preparation of nanocrystals with varied shapes and sizes [6, 7]. There are fundamentally two different approaches to nanoparticle synthesis, top-down and bottom-up techniques. In the first method, external energy is employed to breakdown material into small particles of nanometre dimensions. Ball milling is one such example of a top-down technique for nanoparticle synthesis. Further, in the field of nanoelectronics, a high-energy electron beam is targeted onto a sample, e-beam lithography, to etch out unwanted materials or particles; it reduces the material to a nanometre dimension. This technology is widely concentrated on lithographic patterning. The bottom-up technology utilises physical and chemical forces for the synthesis of nanoparticles. The gaseous phase method of preparation involves chemical vapour deposition (CVD) and physical vapour deposition (PVD). These methods minimise the formation of organic side-products. However, the

requirement of vacuum environment renders this these deposition techniques expensive. Besides that, wet-chemical synthesis has attracted the most number of attentions due to its relatively simplistic and economical approach. Here, the chemical reduction of reaction precursors by thermal decomposition is widely used. Several kinds of metal and metal oxide nanoparticles have been synthesised by this synthesis procedure [8]. In principle, it is the chemical reduction of metal precursors at an elevated temperature where metal ions is reduced to 0 oxidation states (e.g. Zn^{2+} to Zn^0). Additionally, the surface of synthesised nanocrystals can be coated by long-chain organic molecules or polymers during or after the synthesis. This is carried out to achieve monodisperse particles in liquid media [9, 10]. These surfactants form layers on the nanocrystals and further prevent agglomerations and provide colloidal stability. The other important roles played by them are- stopping uncontrolled growth of nanoparticles, and they are also key to achieving different morphologies of nanocrystals like nanorods, nanowires, nanocubes etc. [11, 12].

Doping is another important feature of a semiconductor nanoparticle. It is the addition of impurities to a crystal lattice for altering and manipulating the optical and electrical properties of a nanocrystal. Depending upon the requirement and applications of synthesised nanocrystals, doping levels can be achieved. The colloidal nanocrystals can then be further processed into blending with a conjugated polymer. This nanocomposite solution is used in the fabrication of organic electronics such as polymer light-emitting diodes (PLEDs), organic photovoltaics (OPVs) [13].

1.2 Liquid-phase synthesis of metal oxide nanoparticles

The liquid-phase synthesis of nanomaterials is a widely used method mainly due to its processibility and reproducibility. Nucleation and growth are the two basic steps in the wet-chemical synthesis of nanoparticles. Knowledge regarding the mechanism for the synthesis of nanoparticles is crucial in regulating the size and morphology. However, for several reaction systems, the mechanism is not understood unambiguously. Many theories like LaMer mechanism, Ostwald and Digestive ripening and Finke-Watzke two-step mechanism have been proposed to explain the nucleation and growth of nanoparticles in a solution [14–16].

As briefly mentioned earlier, the synthetic route offers a wide range of versatility in controlling, to some extent, the size and morphology of the synthesised nanoparticles. In order to achieve that, the reaction parameters play a vital role in engineering the desired characteristics of the nanocrystals. Several liquid-phase synthesis methods are available in the literature like, co-precipitation method [17], hydrothermal [18], solvothermal [19], sol-gel [20], polyol [21, 22]. These synthetic methods produce nanoparticles with high crystallinity as the reaction is conducted at the high-temperature condition.

With regard to the ZnO based nanoparticle systems studied in this work, synthesis of undoped ZnO nanopowders and its doped counterparts with modified

band gap is of special interest. Zinc oxide (ZnO) is a versatile semiconductor nanoparticle material attracting many researchers. The wide direct bandgap (3.3 eV) and large excitons binding energy at room temperature (60 meV) enable it to be applicable for many applications. Moreover, the optical and electrical properties of the nanoparticle can be tuned by the addition of impurity into the ZnO crystal structure. Doping ZnO with different types of elements opens up more possibilities of tuning its characteristics and fitting it with the applications accordingly. Metals as dopants for ZnO have drawn interests due to its relative simplicity and versatility that have found applications in optoelectronic devices [23], solar cells [24], gas sensors [25], etc. On top of that, doping of ZnO with transition metal ions is beneficial due to its thermal and chemical stability. Therefore, doping of the semiconductor nanocrystallite with iron alters its magnetic, optical and electrical properties. Doping ZnO semiconductor nanoparticles with trivalent (Al^{3+}, Ga^{3+} and In^{3+}) atoms from the 13th group enhances its optical properties [26, 27]. There are several reported works on the synthesis of ZnO nanoparticles doped with these group 13 elements[28]. Aluminium-doped ZnO nanoparticles, in general, has found many applications as gas sensors [29], catalysts [30], electrode [31] etc. The doping of ZnO with Al is an n-type doping as it creates deficiency of valence electrons. This, in turn, increases the number of charge carriers, which is beneficial for application in optoelectronic devices like solar cells and organic light-emitting diodes.

1.3 Microwave synthesis of nanoparticles

The use of microwave irradiation in chemical synthesis was first reported in 1986 by Richard Gedye *et al.* [32]. They used a microwave reactor to synthesise organic compounds. Since then, this technology has rapidly increased to most areas of synthetic chemistry, nanoparticle synthesis, in particular. It paved a new way to efficiently synthesise metal oxide, metal sulphides, metal selenides nanoparticles etc. [33, 34]. One of the main advantages of using microwave irradiation over conventional heating is the rapidness with which a reaction occurs. Apart from this, the yield of the product is higher and side reactions are avoided.

The principle of this technology is based on the absorption of the radiation in a suitable frequency range for efficient conversion of the electromagnetic energy into heat. Generally, the frequency range of the microwave irradiation is 0.3 to 300 GHz. This electromagnetic radiation has the main applications in radio technology. Moreover, commercial and domestic microwave reactors operate at the frequency of 2.45 GHz, thus, avoiding interference of the frequency bands.

Microwave synthesis of organic compounds is quite popular, but the wet synthesis of nanoparticles is not well-established yet. As stated earlier, the heating in the microwave synthesis is different from conventional heating, like oil bath, as the heating is uniform and efficient. Apart from this, shorter reaction time and good yield are the other two advantages of synthesising nanoparticles with

microwave reactor [21]. Conventional heating is not as effective as the microwave reactor as it heats the walls of the reactor or apparatus and then the reactants by conduction or convection, Fig. 1.1. As a result, the reactants take a longer time to heat up, leading to non-uniform heating of the reactants. The illustration below compares the conventional heating with microwave heating with respect to time.
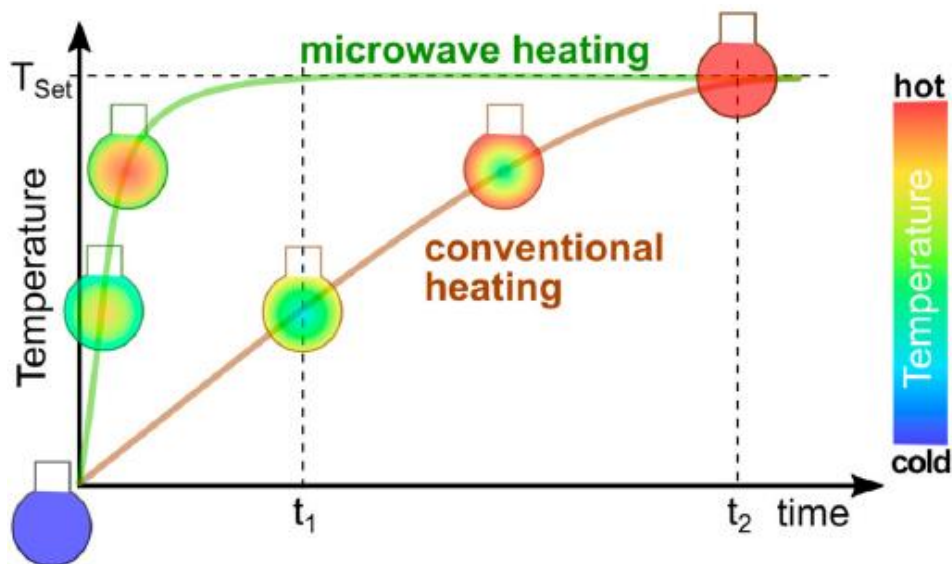
Fig. 1.1 Difference between conventional and MW-heated reaction as a function of time (t1<<t2) [35].

The microwave heating of a matter is based on the absorbing ability of the solvent or reagents. This can be termed as loss tangent or dielectric loss; this is the measure of conversion efficiency of the electromagnetic radiation into heat [36].

The above-described mechanism is an appropriate model for processes in homogeneous phase. The peculiarity of (nano) particle synthesis is the inhomogeneity of the multiphase-system concerning the mechanisms of the radiation absorption and relative permittivity of various phases. It can be hypothesised, that the microwave energy from a constant intensity irradiation source is delivered monotonously to an initially homogeneous reaction system until a critical point when the phase composition of the system changes and new differently (potentially better) absorbing phase (or interphase) appears. Then, the channel of energy dissipation may be changed, and a new dynamics prevails in the system. Such a switching event results in a stepwise process. Examples of suddenly occurring events are already known from hot-spot and run-away phenomena in microwave heating. Unlike these negative phenomena, a beneficial transition step may result in high-quality of the product due to simultaneous triggering of a synthetic step. It was observed in the previous work of our research group [37, 38].

1.4 Band gap engineering

The band gap widening and the emergence of the fine structure of the conductive and valence bands in nanoparticles is a size scale phenomenon not observed in bulk crystals. It is a result of quantum confinement of electronic states in the sufficiently small (nano) objects [39]. Hence, it is possible to control the band gap width just by the particle size. Nevertheless, some additional degrees of freedom in control of the density of states, charge carrier concentration and other properties are desirable. Doping of the material represents such a possibility. It is essential for semiconductors that would otherwise be electrically insulating or less conducting. The important role played by dopants in the semiconductor nanoparticle synthesis has generated research on several applications, especially in the fabrication of electronic and optoelectronic devices [40, 41]. The tuning of band gap of semiconducting material is of good research interest as it changes the properties of the semiconductor. In addition, doping of the semiconductor is one way of achieving that. When a dopant is added to the semiconducting nanomaterial, the energy band gap of the nanoparticle is either widened or reduced; depending upon the type of dopant used.

A dopant can only be successfully incorporated into the host crystallite lattice when, during the reaction, the growth of the host crystal and the deposition of the dopant is balanced [42]. The addition of impurity enhances not only the band gap, but also the luminescent properties. In addition, a material is said to be successfully doped only when the dopant replaces the host atoms rather than just getting adsorbed on the nanocrystal surface. A dopant with more than one or more valence electrons than the host atoms is n-type doping, and the one with one less valence electron is p-type doping. Subsequently, n-type doping has more number of electrons as charge carriers, and in p-type doping, holes form the majority of the carriers [43]. Going ahead, the progress in doped nanocrystals would require optimizing the synthetic control of the dopants and study of its phenomena.

1.5 Surface modification

Capping agents are used to control the growth and particle size in this synthesis method [44]. These long-chain organic ligands are the basic component for attaining control over size and shape of nanoparticles. Other than preventing agglomeration of the nanoparticles during synthesis, the surface-coated nanoparticles can also facilitate in acquiring stable dispersion in solvents [45]. These stabilising agents are amphiphilic in nature, having both hydrophilic group (head) and hydrophobic group (tail). The head and tail parts of the molecule are characterised by functional groups. One of the functional groups anchors onto the surface of a synthesised metal or metal oxide nanoparticles. This, in turn, reduces surface energy checking particle or grain growth and formation of clusters. Some of the common functional groups that constitute a part of capping agents are amino (— NH_2), thiol group (—SH), carboxyl group (—COOH), and sulphate

(— OSO$_3^-$) as in sodium dodecyl sulphate (SDS). Many organic molecules have been used to functionalise the reactive surface of nanoparticle [46, 47]. The capping agent can also control the growth and shape of a nanoparticle. Oleic acid, oleylamine, (trioctylphospine oxide) TOPO, (triethanolamine) TEA etc. are some of the examples of the capping agents.

As mentioned, the capping of nanoparticles enables it to disperse in liquid media for further processing due to their interaction with the (liquid) environment. This colloidal dispersion can be used as building blocks for bridging scales from nanoparticles to materials for various purposes. Most importantly, capping agents enable the nanoparticles to disperse in non-polar solvents. In the context of applications of the surface-modified nanocrystals, especially with the solution-processing of the stable dispersion, it has its pros and cons. Looking at the brighter side of it, as discussed in the current topic, the stable dispersion enables it to be applicable in optoelectronic device fabrication [48]. One of the disadvantages of coating the surface, particularly in the device performance, would be the long-chain organic molecules. These molecules affect the device operation, if it forms an insulating (barrier yet monomolecular) layer, thus intervening transfer of charge carriers.

1.6 Nanocomposite and device preparation

Research on electronic properties of nanocomposite materials has been growing due to its potential applications in optoelectronic devices like organic light-emitting diodes (OLEDs) [49] and organic photovoltaic cells (OPVs) [50]. For example, Zhang et al. utilised a one-step microplasma synthesis of Au nanoparticles in PEDOT:PSS/aqueous, (poly(3,4-ethylenedioxythiophene) polystyrene sulfonate) solution at room temperature. This nanocomposite has potential application as fuel-cell electro-catalyst. Similarly, MEH-PPV, poly[2-methoxy-5-(2'-ethylhexyloxy)-1,4-phenylene vinylene], see Fig. 1.2, was mixed with TiO$_2$ and their photoelectrochemical and optical properties were analysed by Habelhames et al. The bulk heterojunction displayed an increase in its performance after the incorporation of TiO$_2$ nanoparticles [28]. The most studied polymer nanocomposite component is the p-type MEH-PPV which imparts hole charge carrier mobility along its polymer chains [51]. In contrast to that, ZnO is an n-type of semiconductor with electrons involved as charge carriers. Therefore, the composites of ZnO nanoparticles and MEH-PPV are advantageous due to the balance they provide in electrons and holes density, respectively [52].

Recent developments have demonstrated that hybrid inorganic-organic systems (n-type ZnO nanoparticles and conductive polymer) are very interesting for UV LED and OLED applications [53, 54]. Important to this work is the fact that a single layer of nanocomposite active layer is more efficient than two separate layers of MEH-PPV and ZnO nanoparticles [55]. The blending of MEH-PPV with ZnO nanoparticles further improves the efficiency of electron injection into the p-type MEH-PPV polymer [49]. Correspondingly, tailoring of the semiconductor

nanoparticles was achieved by doping it with transition metals which helps in tuning the optical properties with improved light efficiency and emission of optoelectronic devices [56].
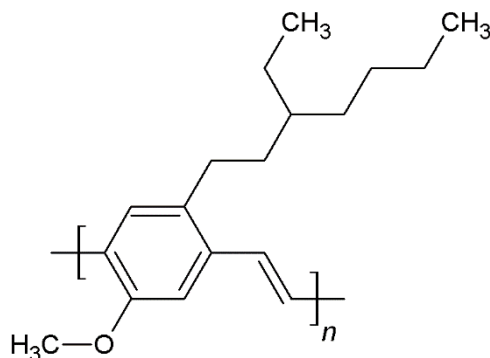
Fig. 1.2 Molecular structure of MEH-PPV.

From the practical point of view, the solution process fabrication of PLED device is economical and is widely researched upon because of its simplicity in comparison to the physical deposition technique where it requires high vacuum condition which is not available in our laboratories. A simple technology of the fabrication of devices is a must under such conditions.

2. AIMS OF THE DOCTORAL THESIS

The thesis focuses on the microwave-assisted polyol synthesis of pure and doped ZnO nanoparticles suitable for application in the fabrication of PLED devices. The aim of the thesis is divided into five specifically addressed points:

1. The first goal is to investigate the effect of minor stoichiometric water content associated with the use of hydrate precursors and the effect of a suitable capping agent in the microwave-assisted polyol synthesis of ZnO nanoparticles. This includes two studies:

    a) Study of the role of the minor water content in the ZnO nanoparticle formation.

    b) Study of the effect of oleic acid employed as a capping agent during nanoparticle synthesis.

2. In the second goal, the effect of the different molar concentration of zinc precursor on the final product properties in the microwave-assisted polyol synthesis of ZnO nanoparticles is to be studied.

3. Thirdly, the goal is to develop a microwave-assisted polyol synthesis of Fe doped ZnO nanoparticle material and characterise the products with specific attention paid to the oxidation state of the dopant. Iron is a transition metal element, and its doping character to ZnO may depend on the preparation method.

4. The fourth goal is in developing a microwave-assisted polyol synthesis of Al-doped ZnO nanoparticle and characterisation of the product. Aluminium belongs to group 13 and is an n-type dopant to ZnO.

5. Finally, the goal is to demonstrate and analyse the performance of PLED diodes using prepared nanoparticles as fillers to the emissive MEH-PPV layer. Neat MEH-PPV polymer-based PLED is used as a reference diode.

3. EXPERIMENTAL METHODS AND INSTRUMENTATIONS

3.1 Instrumental techniques

The synthesis of ZnO and Fe-doped ZnO nanoparticles were carried out in the microwave reactor ERTEC Magnum II (600 W; 2.45 GHz). Following which, EBA 21 Hettich centrifuge was used for separation of the synthesised nanoparticles. To check the crystallinity of the products, XRD peaks were recorded on Rigaku Miniflex 600 with Co K_{α} ($\lambda = 1.7903$ Å) X-ray tube (40 kV, 15 mA). And the average crystalline particle size was calculated using Scherrer's formula, $d = K\lambda/\beta \cos \theta$, where d is the crystallite size, K is a grain shape dependent constant (0.9), λ is the wavelength, θ is a Bragg reflection angle and β is the full-width half-maximum.

The transmission electron microscopy images of the samples were taken on a TEM JEOL JEM 2100 operated at 300 kV (LaB6 cathode, point resolution 2.3 Å equipped with OLYMPUS SYS TENGRA camera (2048 x 2048 pixels). And the particle size distributions were evaluated with Olympus Soft Imaging Solutions software. Also, for the TEM sample preparation, carbon-coated Cu grids (300 mesh) were used where colloidal solutions on the Cu grids were dropped (few μL) and kept for drying for 1 hour at 80 °C. Similarly, the scanning electron microscopy images of the samples were done on a Nova NanoSEM (FEI) microscope with a Schotky field emission electron source (0.02–30 keV) and a TLD detector. The presence of dopants was determined by a scanning electron microscope (SEM) Vega II/LMU (Tescan, Czech Republic) equipped with a backscattered electron (BSE) detector, secondary electron (SE) detector and energy dispersive X-ray (EDX) analyzer (Oxford Instruments INCA). Correspondingly, the hydrodynamic diameters and size distributions were recorded on a Malvern Zetasizer ZS.

The infrared absorption spectra of the powdered samples were studied with FTIR spectra in the region 4000-400 cm-1, Thermo NICOLET 6700 using an ATR technique with a diamond crystal. Further, the absorption spectrometer was performed on a Perkin-Elmer Lambda 1050. DR-UV/Vis measurements were used to study the diffuse reflectance of the powdered samples. Later, from the Tauc plot, the optical band gaps were calculated. And, the emission spectra of the samples were recorded in the photoluminescence (PL) spectra FLS920, Edinburgh Instruments (excitation laser 332.2 nm, Xe lamp excitation 515 nm).

In order to study the electroluminescence spectra, the measurements were recorded on a UV/Vis spectrometer Avantes Avaspec 2048 using an integration sphere with 50 mm diameter. Finally, the I-V characteristics were measured by a multimeter HP 34401A and a power supply system HP 6038A.

Conversions of the recorded spectra to colour coordinates and plotting of the chromaticity diagrams were performed using the free version of the software ColorCalculator released by OSRAM SYLVANIA. (https://www.osram.us)

3.2 Materials

De-ionised water, zinc acetate dihydrate ($Zn(OAc)_2.2H_2O$, p.a., $M_w = 219.51$ g/mol), anhydrous Zinc acetate ($Zn(OAc)_2$, $M_w = 183.48$ g/mol), iron acetylacetonate ($Fe(III)(Acac)_3$, 99 %, $M_w = 324.31$ g/mol), aluminium acetylacetonate ($Al(Acac)_3$, 99 %, $M_w = 353.17$ g/mol), indium acetylacetonate ($In(Acac)_3$, 99 %, $M_w = 412.14$ g/mol) and MEH-PPV Poly[2-methoxy-5-(2-ethylhexyloxy)-1,4-phenylenevinylene] ($M_w = 40000$–70000 g/mol) were purchased from Sigma-Aldrich. Diethylene glycol (p.a., DEG), oleic acid (OA, p.a. $M_w = 282.46$ g/mol), toluene (p.a.), methanol (p.a.) were purchased from PENTA Czech Republic, and PEDOT:PSS (poly(3,4-ethylenedioxythiophene) polystyrene sulfonate) supplied from Heraeus (CleviosTM P AI 4083).

3.3 Synthesis of undoped ZnO, the role of water and capping agent

3.3.1 General synthesis protocol

In a typical synthesis, $Zn(OAc)_2.2H_2O$ or $Zn(OAc)_2$ was used as the ZnO precursor. The calculated amount of the precursor (3.6 mmol of $Zn(OAc)_2.2H_2O$ and $Zn(OAc)_2$ for all the reactions except for ZnO series), was mixed with 50 ml diethylene glycol (DEG) and eventually with a weighed amount of oleic acid as a capping agent in a Teflon-lined container. Further, the reaction mixture was then put in a microwave reactor, turned on, and the power applied was typically 100 % for 15 min. The temperature raise was sigmoidal up to 250 °C. Later, when the reaction was complete, the white suspension (brownish suspension for Fe-ZnO) for pure and Al-doped ZnO was centrifuged and washed with methanol and dried at 80 °C. In addition, some part of the precipitates from the Teflon container was dispersed in 50 cm^3 of toluene to form a colloidal dispersion.

3.3.2 Role of water molecules

The section focuses on the role of water molecules in the synthesis of ZnO nanoparticles using a microwave reactor. $Zn(OAc)_2.2H_2O$ and $Zn(OAc)_2$ were used as ZnO nanoparticle precursor. Diethylene glycol (DEG) was used as a solvent. Three sets of reactions were performed to functionalise the metal oxide nanoparticle surface. The scheme of the reactions is shown in the table below (Table 3.1), to study the role of water. There are two sets of samples, ZOA and ZNP. The acronym NW means no water (anhydrous acetate); CW means crystal water (dihydrate acetate) and 2 or 4 means addition of water to the reaction mixture in the stoichiometry equivalent amount 2 or 4, respectively. Another three sets of reactions were performed to study the role of oleic acid in ZnO nanoparticle synthesis, which is described in the subsequent section.

Table 3.1 Scheme of reactions to study the role of water and oleic acid.

Sample name	ZnO precursor	Water	Oleic acid
ZOA-CW	$Zn(OAc)_2.2H_2O$	Yes	Yes
ZNP-CW	$Zn(OAc)_2.2H_2O$	Yes	No
ZNP-NW	$Zn(OAc)_2$	No	No
ZOA-NW	$Zn(OAc)_2$	No	Yes
ZNP-4W	$Zn(OAc)_2 + 4H_2O$	Yes	No
ZOA-4W	$Zn(OAc)_2 + 4H_2O$	Yes	Yes

3.3.3 Role of capping agent

For the application of nanoparticles, control in the size and morphology of nanoparticle is essential. The functionalisation of the surface of the nanoparticles enables stability to the nanoparticles and regulate growth and final particle size [57, 58]. In the absence of a surfactant, nanoparticles would form a continuous phase. Moreover, proper knowledge and understanding of the role played by a surfactant would open ways to manipulate the size and morphology of a nanoparticle by selectively choosing the right surfactant and varying its molar concentrations. In this work, three sets of reactions were performed to functionalise the metal oxide nanoparticle surfaces by oleic acid (OA). The scheme of the experiments is shown in the table above, Table 3.1. Like the previous reactions, diethylene glycol (DEG) was used as a solvent, and the reaction conditions were as it was in section 3.3.1.

3.3.4 ZnO nanoparticles with different particles sizes

Table 3.2 Reaction scheme of ZnO nanoparticles at varied ZnO molar precursor concentrations.

Sl no.	Sample name	ZnO precursor	ZnO precursor molar conc. (mol/dm^3)	Capping agent
1	ZnO-1	$Zn(OAc)_2.2H_2O$	0.02	OA
2	ZnO-2	$Zn(OAc)_2.2H_2O$	0.04	OA
3	ZnO-3	$Zn(OAc)_2.2H_2O$	0.08	OA
4	ZnO-4	$Zn(OAc)_2.2H_2O$	0.16	OA

In this set of reactions, ZnO nanoparticles were prepared from different molar concentrations of $Zn(OAc)_2.2H_2O$ (1 mmol, 2 mmol, 4 mmol and 8 mmol in 50 mL of the solvent),Table 3.2. The reactions were continued as described in the above-mentioned synthesis.

3.4 Synthesis of doped ZnO

Addition of impurities on the atomic level into the host phase is expected to modify the absorption and fluorescence property of ZnO nanoparticles. Variation in the optoelectronic properties is observed in the semiconductor nanoparticles [40, 59, 60]. The synthesis procedure is the same as mentioned in Section 3.3.1 with the difference in the addition and the amounts of dopants used prior to heating in the microwave reactor. For Fe-, and Al-doped ZnO nanoparticles, 1 %, 5 % and 10 % dopants were used and their optical and electrical properties examined. The percentage of doping relates to the degree of the zinc atom substitution in the formula $D_xZn_{(1-x)}O$, where D stands for dopant. Thus, 5 % means x = 0.05 for example. Iron and aluminium acetylacetonates were used as the source compounds for the doping. The labelling of the samples are as follows: Fe-1 Z, Fe-5 Z, Fe-10 Z, Al-1 Z, Al-5 Z and Al-10 Z for 1%, 5% and 10 % for Fe and Al dopants respectively, Table 3.3.

Table 3.3 ZnO nanoparticles synthesis doped with Fe, Al and dopants.

Sl no.	Sample name	Dopant	Dopant (%)	Capping agent
1	Fe-1 Z	Fe	1	OA
2	Fe-5 Z	Fe	5	OA
3	Fe-10 Z	Fe	10	OA
4	Al-1 Z	Al	1	OA
5	Al-5 Z	Al	5	OA
6	Al-10 Z	Al	10	OA

3.5 Fillers in a conjugate polymer

In the preparation of nanocomposite, a dispersion obtained firstly is as follows, 10 mg of MEH-PPV polymer was dissolved in 3.5 ml of ZnO, Fe- Z, and Al- Z series of nanocolloidal solutions containing 10 mg of nanoparticle powder so that the polymer-to-nanoparticle ratio was 1:1 by weight. The solutions, ZnO/MEH-PPV, $Fe_xZn_{1-x}O$/MEH-PPV, and $Al_xZn_{1-x}O$/MEH-PPV were subjected to ultrasonic treatment and stirred overnight for obtaining fine dispersions. The prepared mixture was used as a precursor for thin film preparations by spin coating the solution on an ITO-coated glass substrate at 800 rpm for 15 seconds.

The samples were then kept for drying in a vacuum oven at 100 °C for 2 hours. The solutions can be identified as, continuing from the previous notations, by adding letters ME (e.g. ZnO-1 ME for undoped ZnO nanoparticles and, Fe-1 ZME, and Al-1 ZME for Fe-doped and Al-doped respectively). Also, for comparison purpose, thin films were prepared from neat MEH-PPV.

3.6 PLED device fabrication

The compositions of the PLED device are electrodes (anode and cathode), hole-transporting layer (HTL) and an active layer. Indium tin oxide (ITO) is the anode that injects holes through an HTL layer made from (PEDOT:PSS) into the active layer from ZnO/MEH-PPV or doped ZnO mixed with MEH-PPV. Electrons are injected to the active layer from Mg cathode deposited on the top of the device structure. The scheme of the device is depicted in Fig. 3.1. As in the previous samples, the notations for the PLED device for ZnO, Fe-ZnO and Al-ZnO are represented as ZnO-1/MEH-PPV, Fe-1 Z/MEH-PPV and Al-1 Z/MEH-PPV respectively.

Spin coating (Laurell WS-650-MZ-23NPP) method was used to prepare thin films of nanometer size thicknesses. In the device fabrication process, the HTL layer (PEDOT:PSS) was coated on a pre-patterned ITO-coated glass substrate to obtain a homogenous thin film. Later, the prepared nanoparticle dispersions (ZnO/MEH-PPV) were deposited onto the HTL layer by spin coating at 1000 rpm and dried in a vacuum oven at 150 °C in order to prepare the active layer. It is then followed by the sputtering of magnesium on the top of the layered structure. An instrument used for sputtering was Quorum Technologies Q300TT. Finally, the device was encapsulated by epoxy resin in order to protect the deposited layers from moisture and prevent contamination. The fabrication of the polymer light-emitting diode (PLED) was performed in a glove box JACOMEX GP Concept, keeping a relative partial pressure of H_2O and O_2 below 10 ppm.
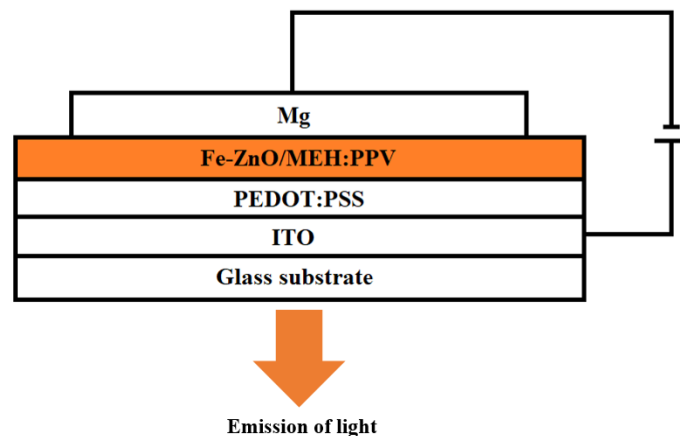

Fig. 3.1 Schematic diagram of Fe-doped ZnO PLED device [61].

4. RESULTS AND DISCUSSIONS

The results and discussions are organised into sections according to the fivefold aims of the thesis. The first four chapters represent original research on nanoparticle synthesis and properties, while the fifth chapter is added to demonstrate the application potential of the synthesised particles in LEDs.

4.1 Undoped ZnO nanoparticles, the role of water and capping agent

In the first study, the role of water molecules in ZnO nanoparticle synthesis was analysed. Here, water molecules play a significant role as they assist the hydrolysis of the zinc precursor (zinc acetate) in the initial stage of the process. The particle nanocrystallite size (as obtained by XRD) increases with the equivalent amount of water, Fig. 4.1.
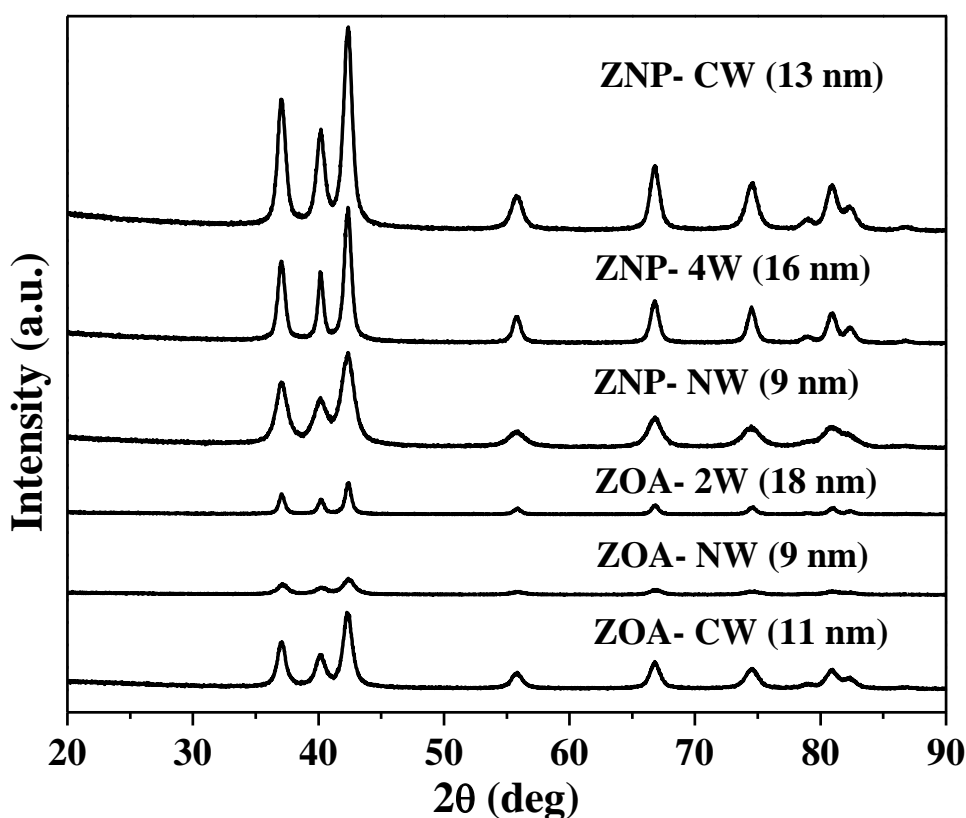
Fig. 4.1 XRD diffractogram of ZnO nanoparticles.

The size of nanocrystallites obtained from XRD measurement can be compared with the TEM images in Fig. 4.2. The ZnO nanoparticles prepared from an anhydrous precursor exhibited the smallest size (9 nm). The size was increased in the case of ZnO nanoparticles prepared from dihydrate precursor (13 nm). The biggest nanoparticles were obtained from the anhydrous precursor with the addition of 4 molar equivalents of H_2O (16 nm). Thus, the water molecule

controls the ZnO nanoparticle size during the synthesis. The water molecule is either supplied *in situ* from the hydrated metal precursor or from the organic medium. The intentional addition of water to DEG solvent was demonstrated as a viable method for synthesised nanoparticle size adjustment.
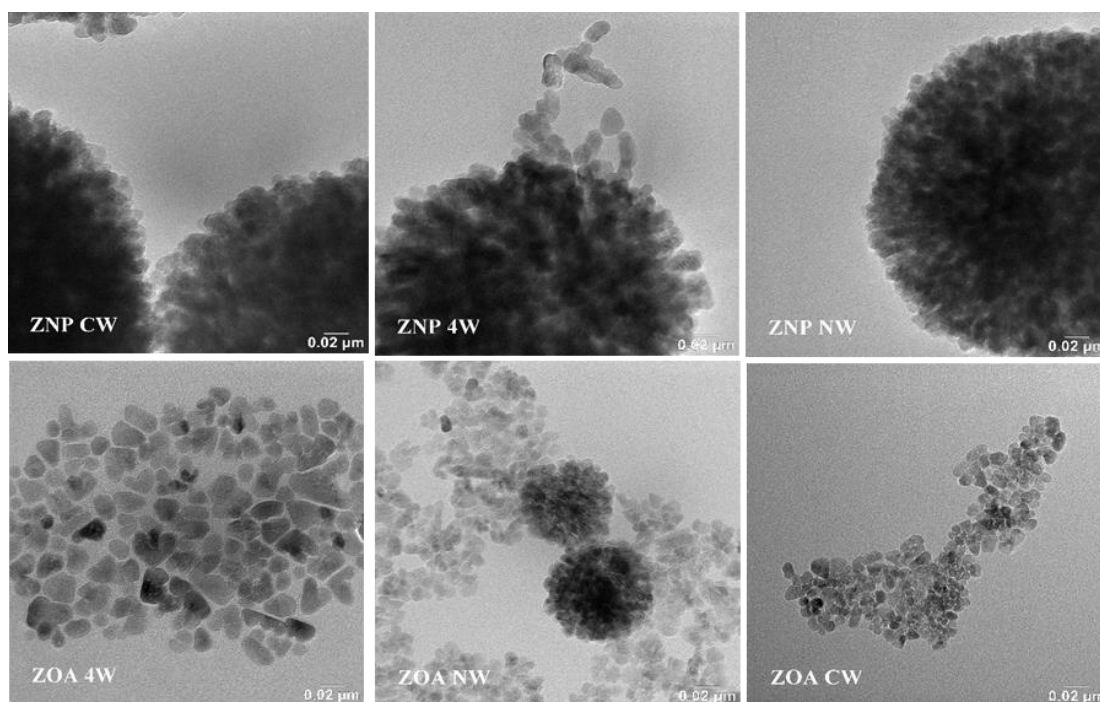
Fig. 4.2 Analysis of water and oleic acid on different ZOA and ZNP samples observed in TEM images.

The spectral properties can be controlled as well because they depend on the particle size. With respect to the employment of the capping agent, OA enabled stable colloidal dispersion of ZnO in toluene. The thickness of an OA monolayer shell on the surface of the particles can be estimated in the range 2-3 nm. Nevertheless, this organic layer does not interfere XRD based estimation of the particle size. The diameter of ZnO nanocrystallites stabilised by OA varied from 9 nm for particles prepared from anhydrous precursor to 18 nm for particles prepared from an anhydrous precursor with the addition of 4 molar equivalent of H_2O. TEM analysis confirmed the presence of isolated ZnO nanoparticles in the dispersion. When synthesis was carried out in the absence of the capping agent, an unstable suspension in toluene was observed, and TEM analysis revealed the presence of large aggregates of the nanoparticles. Moreover, OA is a barrier for transport of the source ions from the solution to the growing particle surface, which is another size controlling mechanism in the synthesis. It seems that there is a cooperative effect of the presence of water and capping agent in the reaction mixture. As a result, OA was used in synthesis throughout the rest of the work.

4.2 ZnO nanoparticles with different precursor molar concentration

ZnO nanoparticles with different particle sizes come with varied properties. The other set of samples (ZnO-1, ZnO-2, ZnO-3 and ZnO-4) are undoped ZnO prepared with different ZnO precursor molar concentrations, Table 3.2

The second series of reactions studied size variation of ZnO nanoparticles by changing the molar concentration of the precursor to find the most proper size for further application in PLED. With increasing molar precursor concentration, the average particle size of ZnO increased in the range from 4 nm to 14 nm (as estimated from TEM images, see Fig. 4.3) for the molar precursor concentrations from 0.02 mol/dm^3 to 0.16 mol/dm^3. The sample with the smallest particle size exhibited the lowest crystallinity and broadest size distribution judging according to all of its characteristics.
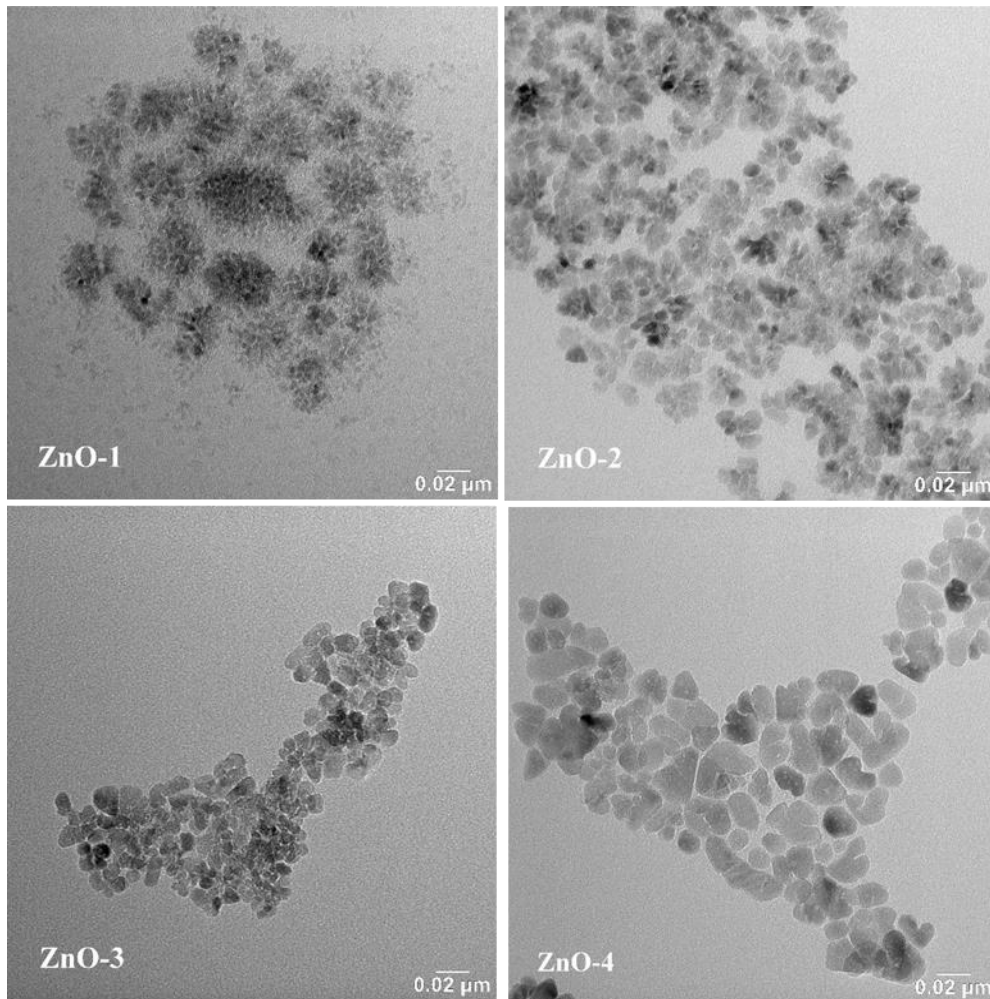
Fig. 4.3 TEM micrographs of ZnO samples [62].

The observed dependence of spectral features on the nanoparticle size correlated well with the prediction by the theoretical Brus equation model. The room temperature PL spectra and normalised peaks, inset, of ZnO samples are

shown in Fig. 4.4 (excited by a laser at 332 nm). The spectra observed at 370-380 nm is attributed to UV near-band-edge emission due to excitonic recombination. Moreover, the peaks also shift to higher wavelength (red-shift) as the particle size is increased. UV-Vis absorption characteristics and results obtained by the PL measurements are summarised Table 4.1.
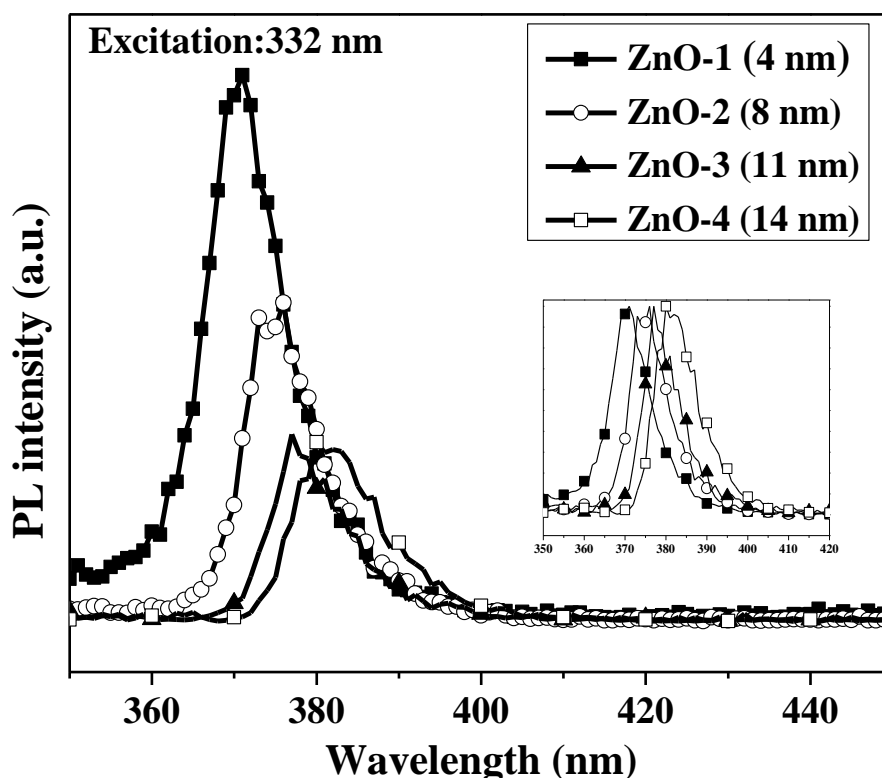
Fig. 4.4 Room-temperature fluorescence spectra of ZnO colloidal samples (inset: normalised peaks) [62].

Table 4.1 Table showing the spectral characteristics of ZnO samples..

Sample	Avg. particle size (nm)	Experimental values				
		UV-Vis λ_{max} * (nm)		$E_{g(Tauc\ plot)}$ (eV)	UV-Vis λ_{edge} ** (nm)	PL emission λ_{max} * (nm)
		M	1'			
ZnO-1	4±3	332	330	3.38	367	370
ZnO-2	8±2	350	345	3.34	371	375
ZnO-3	11±1	353	346	3.33	372	378
ZnO-4	14±3	354	350	3.32	373	380

* M - manual reading and 1'- first derivative method of λ_{max} reading.

** The wavelength was calculated from E_g, as estimated from the Tauc plot.

The stable dispersions of the prepared ZnO nanoparticles in toluene (due to OA) allowed mixing of the particles with MEH-PPV dissolved in toluene. Thus, homogenous thin nanocomposite films were fabricated easily by one-step spin-coating technique. It was confirmed that the addition of 50 wt% of ZnO nanoparticles does not deteriorate the polymer luminescence and, no luminescence attributable to the ZnO nanoparticles is visible when the sample is excited by UV light (332 nm). The incorporation of the nanofillers influences the ordering of the polymer chain favouring the intermolecular interaction slightly over the intramolecular one.

4.3 Fe-doped ZnO nanoparticles

As a third study, band gap engineering of the semiconductor nanoparticles by doping it with metal impurities was investigated. Iron was the metal dopant employed in this section.
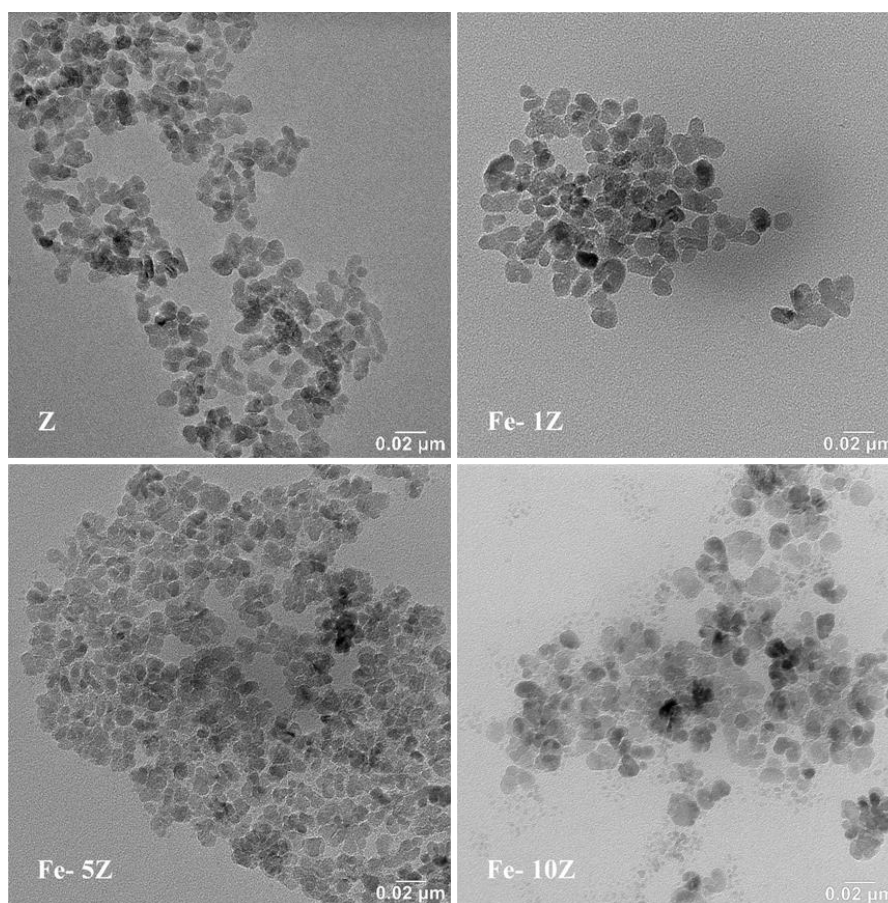
Fig. 4.5 TEM micrograph of Fe-ZnO samples [61].

To modify optical properties, band gap width, and electrical properties of ZnO, the semiconductor nanoparticle was doped with iron. Sample names for Fe-doped ZnO are Fe-1 Z, Fe-5 Z and Fe-10 Z for 1%, 5% and 10% Fe doping respectively. Z is the reference undoped ZnO sample prepared under the same conditions.

The Fe dopant did not influence the average particle size of the nanoparticle much as it is clear from TEM images and XRD analysis, see Fig. 4.5 and Fig. 4.6. Incorporation of the dopant was also confirmed by EDX spectroscopy analysis. Further, it is clear from the XPS spectra that the Fe dopant was present mainly in Fe^{2+} oxidation state. Thus, the reduction of the source ions from Fe^{3+} to Fe^{2+} proceeded during the synthesis which can be explained by the mild reducing effect of DEG. Next, the Fe-doping caused variations of the absorbance and fluorescence spectra of ZnO nanoparticles. Red-shift of the absorption edge was observed with an increase in doping concentration. The band gap varied from 3.2 eV (for undoped sample) down to 2.5 eV (for ZnO doped with 10 % Fe). On the other hand, the increase in doping level was accompanied by the vanishing of the first absorption maxima around 350 nm. Moreover, the Fe-doping has a negative effect on the intensity of the UV peak in the fluorescence emission spectra excited at 332 nm. Thin nanocomposite films with MEH-PPV matrix were prepared from toluene dispersion. The addition of doped nanoparticles did not cause any pronounced change of the polymer photoluminescence emission intensity. On the other hand, the incorporation of the nanofillers had a similar effect on the intra- and inter-molecular interactions of polymer chains as in the case of undoped ZnO.
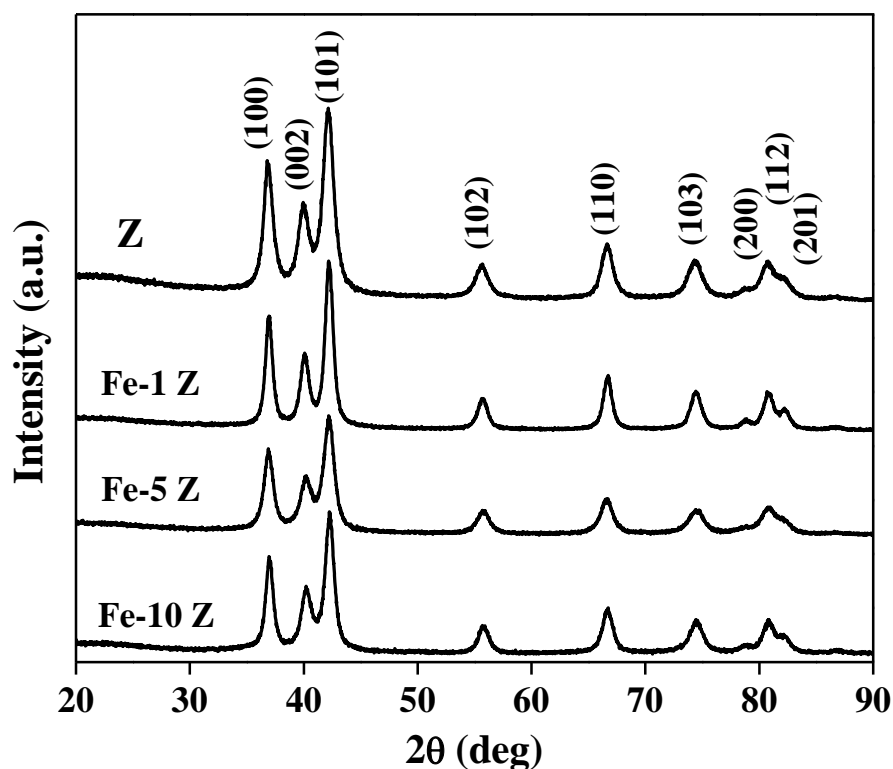

Fig. 4.6 XRD diffractogram of ZnO and Fe-ZnO nanoparticles [61].

The atomic percentage of the elements Fe and Zn were quantitatively analysed by the spectroscopic analytical instrument integrated in SEM. The powdered Fe-doped ZnO samples were calcined at 400 °C prior to the analysis. The obtained concentrations of these atoms were compared with the elemental composition

calculated from initial precursor concentrations and studied, as presented in Table 4.2. The composition of the prepared doped nanoparticles complies with the initial precursor load. A conclusion can be drawn that the EDS and XRD data confirm the presence of Fe (yet without specification of its oxidation state) ions in the ZnO host crystal lattice.

Table 4.2 Contents of Zn and Fe according to the synthesis protocol and concentration of Fe in the product as calculated from precursor content and as measured by EDS [61].

Sample	n_{Zn} (mmol)	n_{Fe} (mmol)	$n_{Fe}/(n_{Fe}+n_{Zn})$ (atomic %)	Fe conc. (EDS) (atomic %)
Fe-1 Z	3.56	0.04	1.10	1.90
Fe-5 Z	3.42	0.18	5.19	4.51
Fe-10 Z	3.24	0.36	10.19	9.40
Z	3.60	--	--	--
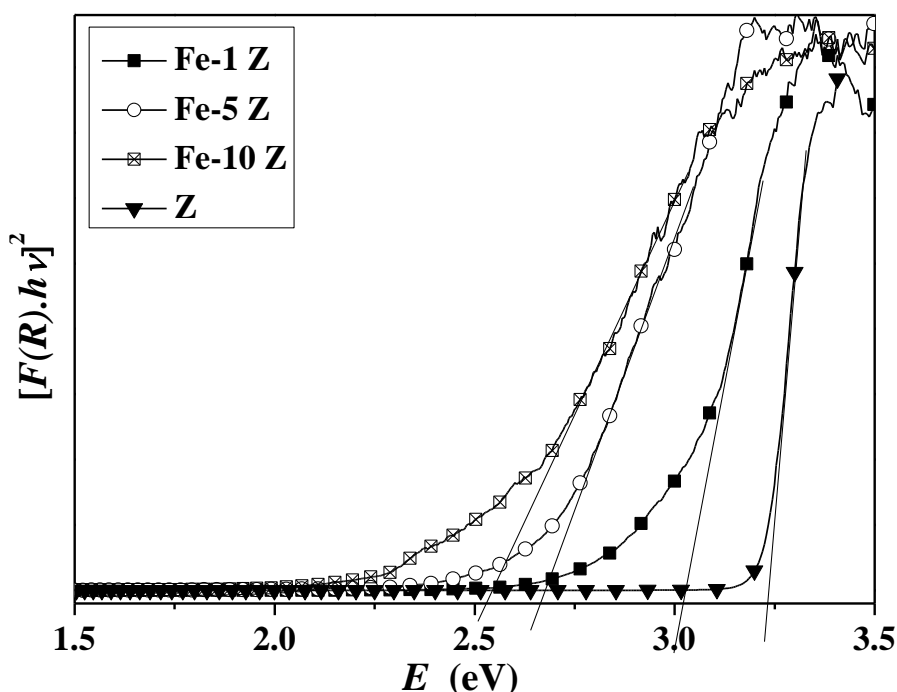
Fig. 4.7 Tauc plot and DRUV-Vis of ZnO and Fe-ZnO powders [61].

The analysis of the absorption band edge of ZnO and Fe-ZnO powdered samples was conducted using diffuse-reflectance ultraviolet-visible spectroscopy (DRUV-Vis), Fig. 4.7. Tauc plot calculation from the absorption region of the diffuse reflectance led to the determination of bandgap of the samples. Pronounced red-shift in absorption spectra with increasing dopant concentration is visible from the Tauc plot clearly. Since the average particle size of the

24

nanoparticle did not change significantly, the shift to longer wavelength is primarily due to the addition of Fe [63, 64].

The photoluminescence (PL) spectra for diluted $Fe_xZn_{1-x}O$ nanoparticle dispersions were investigated as well. With increasing doping concentration, the PL intensity correspondingly reduced. The lowering of the intensity is due to the presence of Fe ions that provides an alternative pathway for the relaxation of excited electrons. Since no peaks were observed in the visible region for undoped and Fe-doped ZnO, all transitions related to the corresponding states in the band gap are non-radiative. Besides, the surface functionalisation of the nanoparticle surface by oleic acid led to the absence of luminescence corresponding to surface defects [65].

The oxidation state of Fe in Fe-doped ZnO nanoparticles characterised by XPS. An example of the high resolution XPS spectra is shown in Fig. 4.8. The core peak positions of Fe $2p_{1/2}$ and Fe $2p_{3/2}$ are 709.8 and 723.5 eV, 710.1 and 723.9 eV for 1 and 5 % respectively. The satellite peak was recorded at 716.3 and 729.8 for 1 % and 717.6 and 731.9 eV for 5 %. Besides, the binding energy difference of Fe $2p_{1/2}$ and Fe $2p_{3/2}$ is around 13 eV. These peaks were deconvoluted into two peaks to distinguish the oxidation state of Fe^{2+} and Fe^{3+}, The values were in coherence with the work published by Karamat *et al.* [66]. Concerning quantification, Fe^{2+} was identified as the prevailing form in the sample. Besides that, the presence of Fe^{3+} is manifested in the spectrum. However, precise quantification is not possible with respect to the relatively poor resolution.
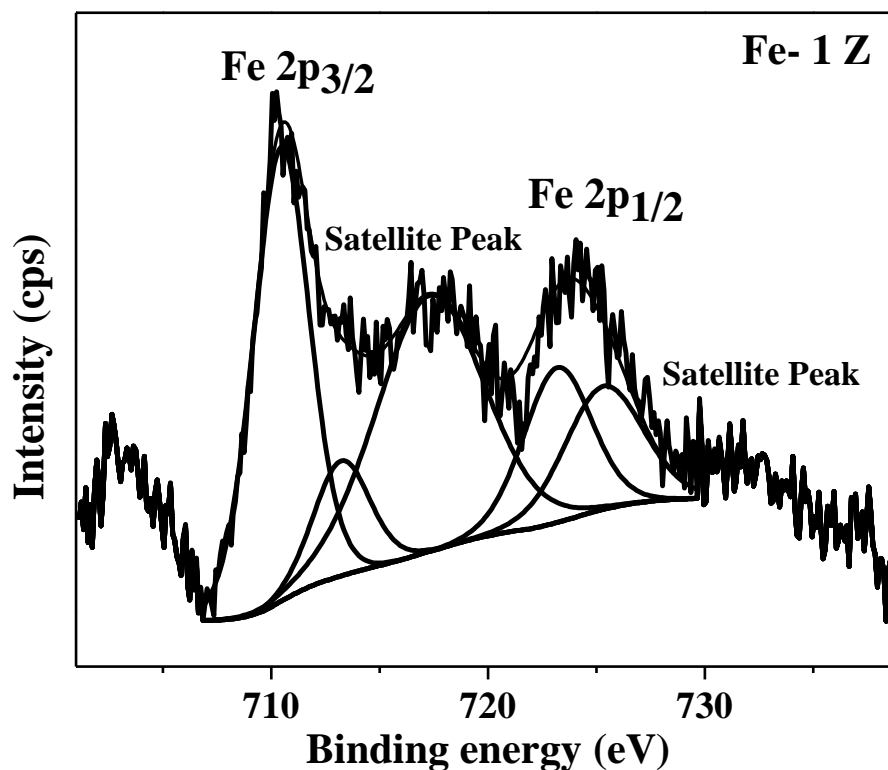

Fig. 4.8 Narrow scan XPS core spectra of Fe 2p of the $Fe_xZn_{1-x}O$, sample x=0.0 [61].

4.4 Al-doped ZnO nanoparticles

In the fourth study, the ZnO nanoparticles were doped with a trivalent dopant Al (p-block element) using similar concentrations as in Fe-doped ZnO samples. To modify optical properties, band gap width, and electrical properties of ZnO, n-doping by aluminium was investigated as the second choice of dopant. The synthesis of Al-ZnO was explored by varying the Al doping concentration. As in Fe-doped ZnO nanoparticles, the same atomic doping concentration was utilised. Sample names for Al-doped ZnO are Al-1 Z, Al-5 Z and Al-10 Z are for 1%, 5% and 10% Al doping, respectively. Z is the reference undoped ZnO sample prepared under the same conditions but without any doping (the same as in section 4.3).

The variation of the particle size with Al doping concentration was not significant, as can be seen from Fig. 4.9. The XRD confirmed single hexagonal wurtzite (ZnO) phase composition of all the samples. Absence of secondary phases of oxides of Al corresponds to the presence of Al^{3+} ions in the host dispersed at the atomic level.
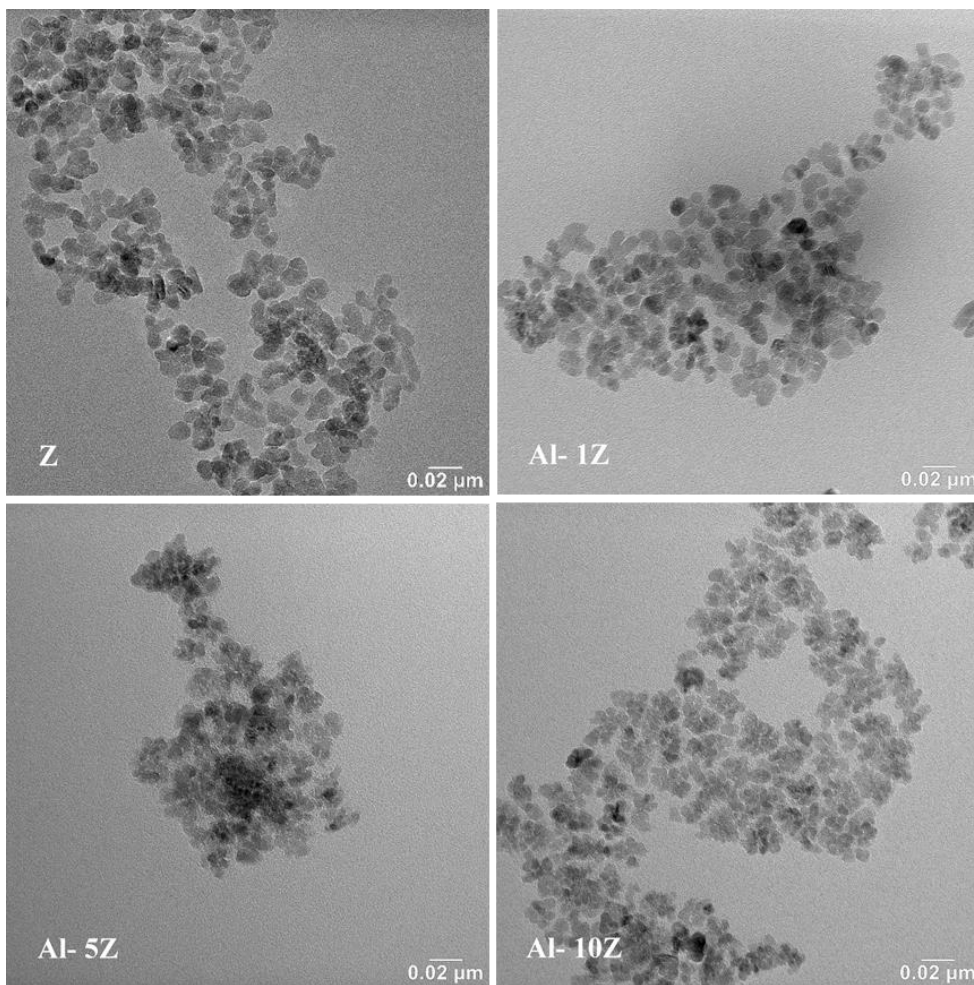
Fig. 4.9 TEM micrograph of undoped ZnO and Al-doped ZnO nanoparticles

The dopant concentration and composition of aluminium-doped zinc oxide was assessed by energy-dispersive X-ray spectroscopy (EDS). From the EDX spectra, Zn, O and Al peaks are observed for the doped samples. The calculated concentrations and the observed values are comparable (Table 4.3).

Table 4.3 Al concentration calculated from amounts of reaction precursors in comparison with Al-dopant concentration as obtained from EDS analysis.

Sample	n_{Zn} (mmol)	n_{Al} (mmol)	$n_{Al}/(n_{Al}+n_{Zn})$ (atomic %)	Al conc. (EDS) (atomic %)
Al- 1Z	3.58	0.05	1.28	1.60
Al- 5Z	3.43	0.18	4.98	5.23
Al- 10Z	3.28	0.37	10.13	9.39
Z	3.60	--	--	--
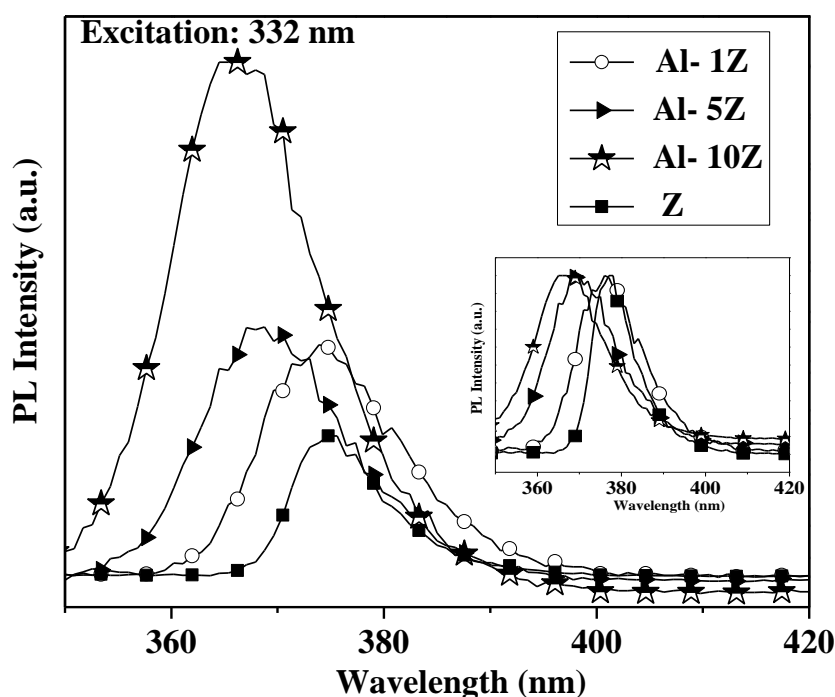
Fig. 4.10 Room temperature PL spectra of pure and Al-doped ZnO colloids [67].

The band gap estimated from Tauc plot was decreased by 0.1 eV in contrast to undoped ZnO nanoparticles but did not vary much with doping concentration. On the other hand, there was a blue shift and an increase in the intensity of the PL emission peak due to the presence of the dopant, Fig. 4.10. The hypsochromic shift (from 377 nm for undoped ZnO to 366 nm for 10 % Al-doped ZnO) indicates broadening of the transition band gap with increasing Al concentration, which is virtually in contradiction with the band gap estimations from UV-Vis absorption

spectra. It could be that, not only new states are created below the conduction band of ZnO, but also the lowest states in the conduction band are partially filled by the electrons from the dopant. The filling of the lowest states in the conduction band of ZnO by electrons from the dopant may result to higher energy of radiative recombination transition (Burstein-Moss shift) while the shallow states can be more manisfested in the Tauc plot [38].

Thin nanocomposite films with MEH-PPV matrix were prepared from toluene dispersion, and the addition of doped nanoparticles yielded similar results as in the previous two studies. It can be concluded that, the observed features are due to the incorporation of the nanofillers. It is a general effect of the nanocomposite formation, and no specific manifestations of particle doping were observed in the PL spectra.

4.5 Proof-of-concept PLEDs

The last part of the dissertation was focused on the demonstration of the potential of synthesised particles as fillers for nanocomposites applicable in electronics. PLEDs using synthesised nanoparticles embedded in MEH-PPV polymer matrix were prepared and studied within the framework of another dissertation run in the research group [68]. This previous study was focused on detailed analysis of mechanisms and the role of the nanoparticles in the prepared devices. Here, the fabrication of the PLEDs allowed selecting the optimum size of the nanoparticles first. The best performance of nanocomposite PLEDs was achieved for ZnO nanoparticles of ca 11 nm in diameter. It was also confirmed that the presence of OA surface shell has no detrimental effect on the nanoparticulate filler function in the device. An example of fabricated devices is presented Fig. 4.11.
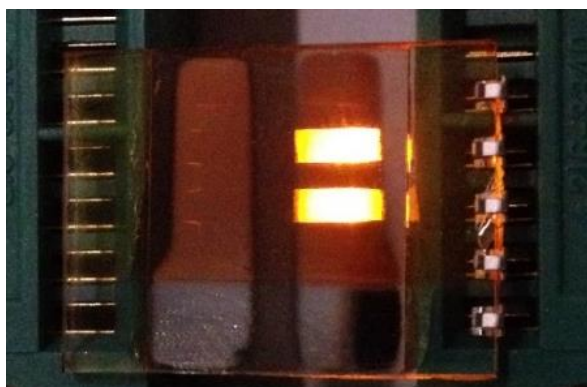
Fig. 4.11 Luminance of two pixels of ZnO-3/MEH-PPV PLED device @ 10 V.

Next, the emphasis was put on further development of the prepared diode characterisation and interpretation of the effects of ZnO nanoparticle addition and its doping. The prepared PLED devices were dealt as a source of coloured light, and the results were viewed from the point of practical application.
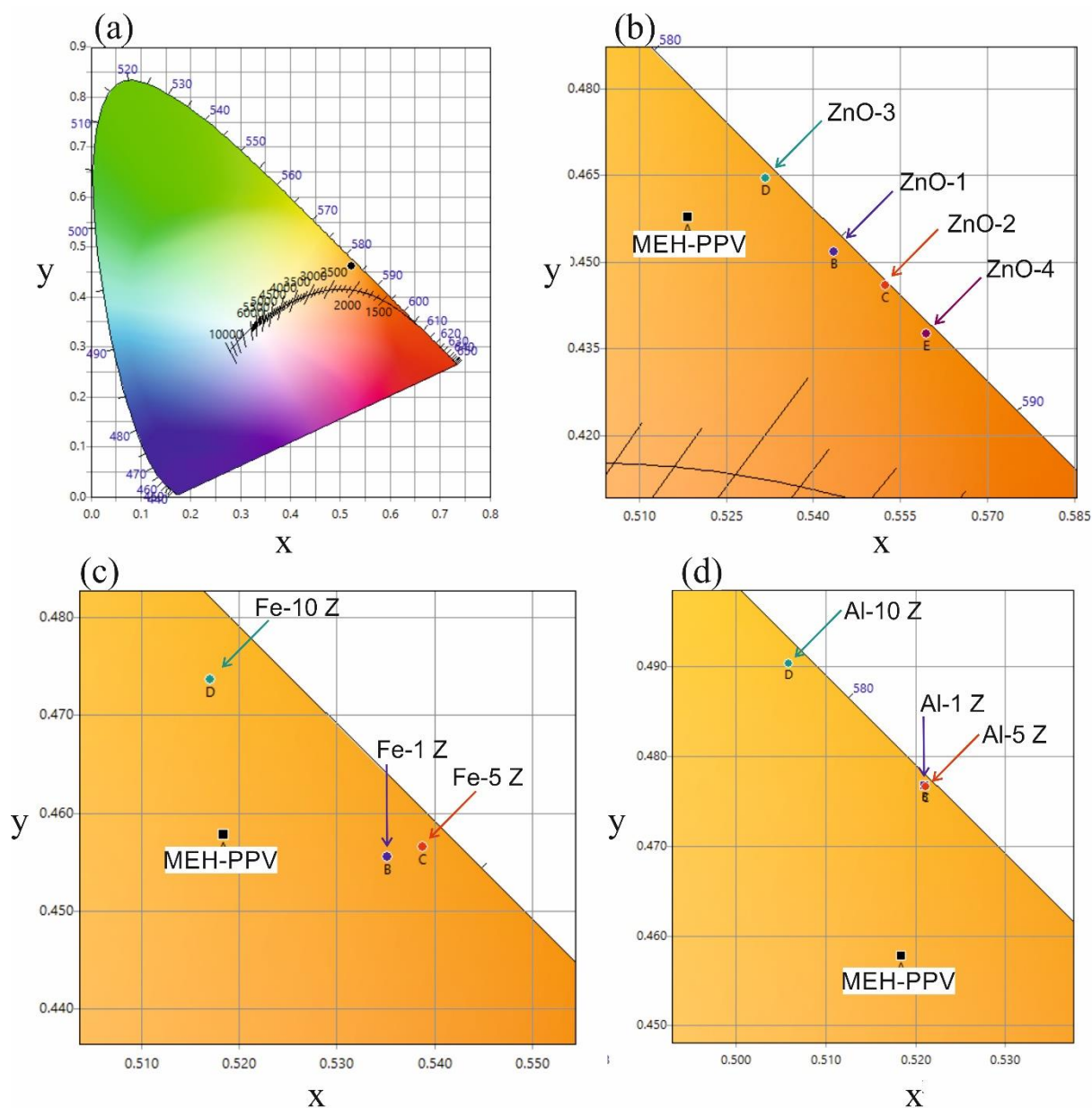
Fig. 4.12 Chromaticity diagram (CIE 1931) of PLED devices with (a) MEH-PPV, (b) ZnO/MEH-PPV (magnified), (c) Fe- Z/MEH-PPV (enlarged) and, (d) Al- Z/MEH-PV (magnified), as active layers.

The CIE 1931 chromaticity diagram of the PLED devices prepared with neat MEH-PPV polymer, ZnO nanofilers (undoped and doped) is depicted in Fig. 4.12. A PLED with the active layer prepared from neat MEH-PPV was used as a reference Fig. 4.12 (a). It emitted a yellowish-orange light of low intensity. The addition of ZnO nanoparticles enhanced the luminance of the PLEDs significantly while the opening voltage was lowered slightly. The chromaticity of ZnO/MEH-PPV diodes approached the spectral locus indicating monochromaticity of emitted light Fig. 4.12 (b). Incorporation of Fe doped ZnO nanoparticles to the active layer affected the opening voltage much more positively; however, it is at

the expense of the electroluminescence intensity. Fe is a positive dopant to ZnO. Hence, it contributes to the charge carrier imbalance compared to undoped ZnO counterparts and lowers the efficiency of the diode. The monochromaticity of the emitted light is also not that good as in the case of undoped ZnO/MEH-PPV PLEDs Fig. 4.12 (c). On the other hand, it was found that Al-doping had an extremely positive effect on both the EL intensity and lowering of the opening bias voltage. Al is a negative dopant and contributes positively to the charge carrier balance in the diode. The application of Al-doped nanoparticles resulted in the shift of the emitted light to the yellow gamut very close to the spectral locus Fig. 4.12 (d). The best performing Al-doped ZnO MEH-PPV PLED was about 14 times brighter than the neat MEH-PPV reference PLED device.
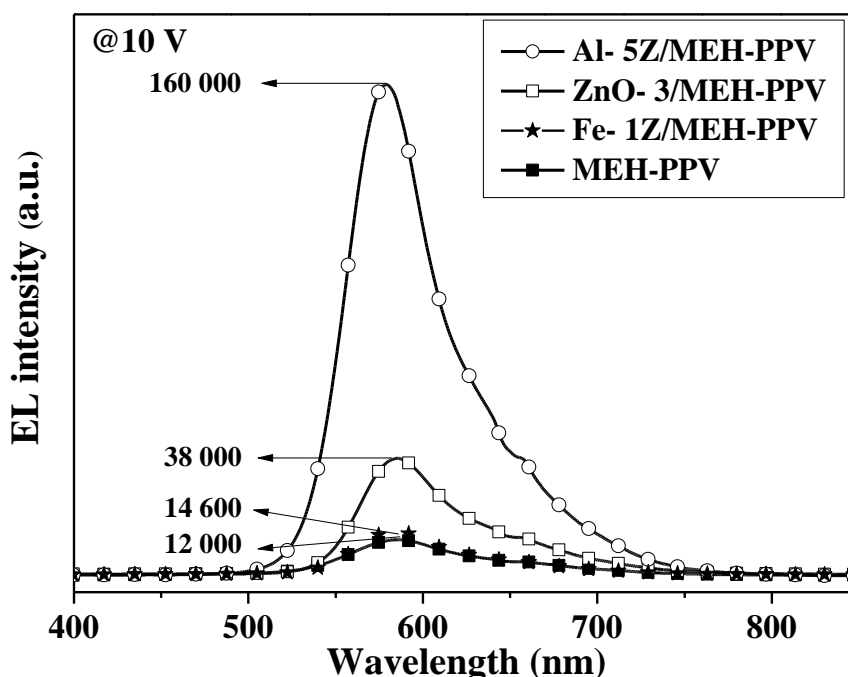
Fig. 4.13 Comparison of the best performing PLEDs from each sample series with the reference diode.

In order to compare the effects of the various nanofillers, the emission spectra of the best performing PLED devices was selected from each sample series, as depicted in Fig. 4.13. Incorporation of undoped ZnO nanofiller increased the luminance of the PLED more than three times comparing with the neat MEH-PPV reference PLED. When the ZnO nanofiller was positively doped by Fe, a decrease of PLEDs luminance was observed for higher doping levels. The best performing sample with the lowest doping level had similar maximum EL intensity as the reference. In contrast to that, n-type Al doping of ZnO increased the PLEDs EL intensity more than thirteen times compared to the reference PLED.

5. CONCLUSION

In this work, the research is focused on the microwave-assisted polyol synthesis of undoped and doped ZnO nanoparticles. The role of water molecules, oleic acid as the capping agent and dopants (Fe and Al) were investigated. Moreover, the prepared ZnO nanoparticles with varied average particle size showed different optical properties. The microwave reactor enabled the rapid and uniform heating of the reaction mixtures. As demonstrated in this work, polyol synthesis is a rapid and efficient preparation technique for obtaining nanocrystalline particles. Since a high boiling point solvent was employed, the reaction was conducted at high temperature, the result being the production of high crystalline nanoparticles within 15 min. Moreover, a stable dispersion of the as-synthesised nanoparticles was possible due to surface modification by the capping agent. The nanoparticles obtained using the microwave reactor were reproducible and highly crystalline. All the particles exhibited a sharp peak in the UV region of the photoluminescence emission spectra. No emission was observed in the visible part of the spectra confirming good crystallinity of the particles and passivation of eventual surface defects. Both the solvent (diethylene glycol, DEG) and the capping agent (oleic acid, OA) have the passivation capability. In order to actualise the potential of the prepared ZnO and doped ZnO nanoparticles, the colloids were blended with a conjugate polymer MEH-PPV, deposited on a substrate by spin-coating technique and their optical properties were studied. Finally, polymer light-emitting diode (PLED) devices were prepared, and their optoelectronic characteristics were analysed. Addition of the ZnO nanoparticles increases the EL emission intensity generally in comparison with the reference neat MEH-PPV diode. It can be explained by the n-type character of ZnO, which improves the charge carrier balance in the p-type MEH-PPV conductive polymer emissive layer. When the ZnO nanofiller was positively doped by Fe, a decrease of PLEDs luminance was observed for higher doping levels. In contrast to that, n-type Al doping of ZnO increased the PLEDs EL intensity largely even compared to the devices with undoped ZnO nanoparticles. With further development in band gap engineering of ZnO nanoparticles, it can be expected that suitable doping allows for even much higher PLED efficiency in the future.

CLOSING REMARKS

Contribution to science and practice

ZnO semiconductor nanoparticles is a widely researched material. The versatility of the material is eminent in various research fields and its applicability in many scientific areas. In addition to that, the characteristics of ZnO nanoparticles can be altered and tailored according to the requirement for various application purposes. In this work, for the preparation of PLED devices, the optical properties of ZnO nanoparticles were tailored for better performance of the devices. Bandgap engineering is one of the ways of achieving it. The intentional addition of foreign metal ions into the host atom alters the optical characteristics of the host crystal lattice. In this work, undoped ZnO and doped ZnO nanoparticles possessed characteristics different from each other due to average particle size, types and concentration of dopants. When ZnO nanoparticles were prepared with different molar precursor concentration, the average particle size of the nanocrystals varied. With the increase in molar precursor concentration, there was an increase in the particle size too. However, when Fe and Al dopants were used to dope ZnO nanoparticles, the particle size differences were not very significant. It, however, altered its optical properties due to the different concentration of the dopants. The absorbance and fluorescence results confirmed the effects of doping on ZnO nanoparticles. The polyol synthesis of undoped and doped ZnO nanoparticles in a microwave reactor provides an efficient and rapid technique to prepare semiconductor nanoparticles. The high boiling point multivalent alcohol is characterised by reduction potential of some metal precursors into metal ions of lower valency state. With the first use of the polyol technique by Fievet, Lagier and Figlarz in 1989 [69], it has since become a reliable method for nanoparticle synthesis. One of the main advantages of the polyol solvent is its ability to solubilise metal precursors during the reaction. The solubility is often considered equivalent to water. This is advantageous as it allows the use of easily-available and economical metal salts as precursors for metal nanoparticles. Even during the synthesis of nanoparticles, the multidentate nature of the solvent leads to a good chelating effect on to the metal salts. This effect usually controls particle nucleation, growth and agglomeration of the final product formed. However, large nanoparticle aggregates were produced in our synthesis. To further elaborate the effectiveness of the polyol solvent, the colloidal stability was improved by utilisation of oleic acid as a capping agent. It delivers stabilising effect by binding carboxyl group to the surface of the nanoparticles. Not only this, surface-modified ZnO, when mixed with conjugate polymer MEH-PPV, brings in a different flavour in terms of application in the fabrication of optoelectronic devices. The nanocomposite of the ZnO-based filler with the conjugate polymer functions as an active/emissive layer in the fabricated PLED device. From the electroluminescence spectra, it was observed that the addition of fillers enhances the luminescent intensity. The

highest luminance was observed in case of Al-doped ZnO. Moreover, Al-ZnO samples related diodes had lower opening voltages (2.8 V) compared to the one with undoped ZnO nanoparticles related PLED diodes (5.0 V). For Fe-doped ZnO based device, the forward bias voltage (2.8 V) was reduced reasonably, when compared with its undoped ZnO nanoparticle analogue (5.0 V) but, it was at the expense of the EL intensity.

The work contributes by delivery of the original knowledge about the role of ZnO precursor concentrations, water and the use of oleic acid as a capping agent in the synthesis of ZnO nanoparticles. Based on the obtained results, it is possible to intentionally alter the size, band gaps and optical properties (3.18 eV to 3.34 eV). Moreover, the electronic properties of ZnO can be tuned by doping. Fe and Al dopants showed different optical characteristics at different dopant concentrations (1, 5 and 10 atomic %). This will help us to rationalise the particle synthesis.

The prepared surface-functionalised ZnO nanoparticles were used for nanocomposite preparation with standard conductive polymer MEH-PPV and thin films made from these materials were used as active layers in the fabrication of PLEDs. It was observed that pure ZnO nanoparticles (fillers) significantly enhanced the luminescence of the devices. The use of Fe-doped ZnO nanoparticles causes depreciation in the EL intensity; however, it lowered the forward bias voltage needed to power the device. Contrary to Fe dopant, doping of ZnO with Al resulted in much higher EL intensity of the devices as well as in lowering of the opening voltage.

Ongoing research and future prospect

Microwave-assisted synthesis of ZnO nanoparticles with varied reaction conditions and dopants were investigated. The polyol reaction method was employed for all the syntheses and optimised in the condition of our research laboratories. The main achievement is represented by the introduction of the microwave-assisted heating of the reaction mixture. Preparation of heavily n-doped ZnO nanoparticles will be the next logical step in the continuation of the present research. Besides Al, In- and Ga-doped ZnO shall be considered.

The work was not confined to synthesis alone, a series of thin-films were cast by spin-coating technique and its optical and electronic properties studied. As an actualisation of the applicability of the synthesised semiconductor nanoparticles, the nanocomposite was cast as an active/emissive layer in the fabrication of PLED devices. Extensive experience of electronic devices fabrication and testing was gained in the research group.

REFERENCES

[1] BOISSEAU, P. and LOUBATON, B. Nanomedicine, nanotechnology in medicine. *Comptes Rendus Physique* [online]. 2011, **12**(7), 620–636. ISSN 16310705.

[2] LEE, J.H., MIRZAEI, A., KIM, J.Y., KIM, J.H., KIM, H.W. and KIM, S.S. Optimization of the surface coverage of metal nanoparticles on nanowires gas sensors to achieve the optimal sensing performance. *Sensors and Actuators, B: Chemical* [online]. 2020, **302**(December 2018), 127196. ISSN 09254005.

[3] PRASAD, R., BHATTACHARYYA, A. and NGUYEN, Q.D. Nanotechnology in sustainable agriculture: Recent developments, challenges, and perspectives. *Frontiers in Microbiology* [online]. 2017, **8**(JUN), 1–13. ISSN 1664302X.

[4] EBRAHIMI, Y., PEIGHAMBARDOUST, S.J., PEIGHAMBARDOUST, S.H. and KARKAJ, S.Z. Development of Antibacterial Carboxymethyl Cellulose-Based Nanobiocomposite Films Containing Various Metallic Nanoparticles for Food Packaging Applications. *Journal of Food Science* [online]. 2019, **84**(9), 2537–2548. ISSN 17503841.

[5] ALVES, T.E.P., KOLODZIEJ, C., BURDA, C. and FRANCO, A. Effect of particle shape and size on the morphology and optical properties of zinc oxide synthesized by the polyol method. *Materials and Design* [online]. 2018, **146**, 125–133. ISSN 18734197.

[6] AN, K. and SOMORJAI, G.A. Size and Shape Control of Metal Nanoparticles for Reaction Selectivity in Catalysis. *ChemCatChem* [online]. 2012, **4**(10), 1512–1524. ISSN 18673880.

[7] KIM, H.J., ROH, D.K., JUNG, H.S. and KIM, D.S. Size and shape control of monoclinic vanadium dioxide thermochromic particles for smart window applications. *Ceramics International* [online]. 2019, **45**(3), 4123–4127. ISSN 02728842.

[8] FIEVET, F., AMMAR-MERAH, S., BRAYNER, R., CHAU, F., GIRAUD, M., MAMMERI, F., PERON, J., PIQUEMAL, J.Y., SICARD, L. and VIAU, G. The polyol process: a unique method for easy access to metal nanoparticles with tailored sizes, shapes and compositions. *Chemical Society Reviews* [online]. 2018, **47**(14), 5187–5233. ISSN 14604744.

[9] WANG, Y. and YANG, H. Oleic acid as the capping agent in the synthesis of noble metal nanoparticles in imidazolium-based ionic liquids. *Chemical Communications* [online]. 2006, (24), 2545–2547. ISSN 13597345.

[10] SHARMA, K.S., NINGTHOUJAM, R.S., DUBEY, A.K., CHATTOPADHYAY, A., PHAPALE, S., JULURI, R.R., MUKHERJEE, S., TEWARI, R., SHETAKE, N.G., PANDEY, B.N. and VATSA, R.K. Synthesis and characterization of monodispersed water dispersible Fe3O4

nanoparticles and in vitro studies on human breast carcinoma cell line under hyperthermia condition. *Scientific Reports* [online]. 2018, **8**(1), 1–11. ISSN 20452322.

[11] CAMPISI, S., SCHIAVONI, M., CHAN-THAW, C.E. and VILLA, A. Untangling the role of the capping agent in nanocatalysis: Recent advances and perspectives. *Catalysts* [online]. 2016, **6**(12), 1–21. ISSN 20734344.

[12] BANDULASENA, M. V., VLADISAVLJEVIĆ, G.T., ODUNMBAKU, O.G. and BENYAHIA, B. Continuous synthesis of PVP stabilized biocompatible gold nanoparticles with a controlled size using a 3D glass capillary microfluidic device. *Chemical Engineering Science* [online]. 2017, **171**, 233–243. ISSN 00092509.

[13] ZHAN, C., YU, G., LU, Y., WANG, L., WUJCIK, E. and WEI, S. Conductive polymer nanocomposites: a critical review of modern advanced devices. *Journal of Materials Chemistry C* [online]. 2017, **5**(7), 1569–1585. ISSN 20507526.

[14] THANH, N.T.K., MACLEAN, N. and MAHIDDINE, S. Mechanisms of nucleation and growth of nanoparticles in solution. *Chemical Reviews* [online]. 2014, **114**(15), 7610–7630. ISSN 15206890.

[15] CHU, D.B.K., OWEN, J.S. and PETERS, B. Nucleation and Growth Kinetics from LaMer Burst Data. *Journal of Physical Chemistry A* [online]. 2017, **121**(40), 7511–7517. ISSN 15205215.

[16] WHITEHEAD, C.B., ÖZKAR, S. and FINKE, R.G. LaMer's 1950 Model for Particle Formation of Instantaneous Nucleation and Diffusion-Controlled Growth: A Historical Look at the Model's Origins, Assumptions, Equations, and Underlying Sulfur Sol Formation Kinetics Data. *Chemistry of Materials* [online]. 2019, **31**(18), 7116–7132. ISSN 15205002.

[17] DE MELLO, L.B., VARANDA, L.C., SIGOLI, F.A. and MAZALI, I.O. Co-precipitation synthesis of (Zn-Mn)-co-doped magnetite nanoparticles and their application in magnetic hyperthermia. *Journal of Alloys and Compounds* [online]. 2019, **779**, 698–705. ISSN 09258388.

[18] KUBRA, K.T., SHARIF, R., PATIL, B., JAVAID, A., SHAHZADI, S., SALMAN, A., SIDDIQUE, S. and ALI, G. Hydrothermal synthesis of neodymium oxide nanoparticles and its nanocomposites with manganese oxide as electrode materials for supercapacitor application. *Journal of Alloys and Compounds* [online]. 2020, **815**. ISSN 09258388.

[19] FOTUKIAN, S.M., BARATI, A., SOLEYMANI, M. and ALIZADEH, A.M. Solvothermal synthesis of CuFe2O4 and Fe3O4 nanoparticles with high heating efficiency for magnetic hyperthermia application. *Journal of Alloys and Compounds* [online]. 2020, **816**, 152548. ISSN 09258388.

[20] LEMARCHAND, A., RÉMONDIÈRE, F., JOUIN, J., THOMAS, P. and MASSON, O. Crystallization Pathway of Size-Controlled SnO2 Nanoparticles Synthesized via a Nonaqueous Sol-Gel Route. *Crystal*

Growth and Design [online]. 2020, **20**(2), 1110–1118. ISSN 15287505.

[21] DONG, H., CHEN, Y.C. and FELDMANN, C. Polyol synthesis of nanoparticles: status and options regarding metals, oxides, chalcogenides, and non-metal elements. *Green Chemistry* [online]. 2015, **17**(8), 4107–4132. ISSN 14639270.

[22] FUJIEDA, S., GAUDISSON, T., GRENÈCHE, J.M., FRANÇOIS, M. and AMMAR, S. Synthesis of magnetic wires from polyol-derived Fe-glycolate wires. *Nanomaterials* [online]. 2020, **10**(2), 3–9. ISSN 20794991.

[23] QIAN, L., ZHENG, Y., CHOUDHURY, K.R., BERA, D., SO, F., XUE, J. and HOLLOWAY, P.H. Electroluminescence from light-emitting polymer/ZnO nanoparticle heterojunctions at sub-bandgap voltages. *Nano Today* [online]. 2010, **5**(5), 384–389. ISSN 17480132.

[24] BEEK, W.J.E., WIENK, M.M. and JANSSEN, R.A.J. Efficient Hybrid Solar Cells from Zinc Oxide Nanoparticles and a Conjugated Polymer. *Advanced Materials* [online]. 2004, **16**(12), 1009–1013. ISSN 0935-9648.

[25] BHATIA, S., VERMA, N. and BEDI, R.K. Ethanol gas sensor based upon ZnO nanoparticles prepared by different techniques. *Results in Physics* [online]. 2017, **7**, 801–806. ISSN 22113797.

[26] MOHANTA, A., SIMMONS, J.G., EVERITT, H.O., SHEN, G., MARGARET KIM, S. and KUNG, P. Effect of pressure and Al doping on structural and optical properties of ZnO nanowires synthesized by chemical vapor deposition. *Journal of Luminescence* [online]. 2014, **146**, 470–474. ISSN 00222313.

[27] BERNARDO, M.S., VILLANUEVA, P.G., JARDIEL, T., CALATAYUD, D.G., PEITEADO, M. and CABALLERO, A.C. Ga-doped ZnO self-assembled nanostructures obtained by microwave-assisted hydrothermal synthesis: Effect on morphology and optical properties. *Journal of Alloys and Compounds* [online]. 2017, **722**, 920–927. ISSN 09258388.

[28] AYDIN, H., YAKUPHANOGLU, F. and AYDIN, C. Al-doped ZnO as a multifunctional nanomaterial: Structural, morphological, optical and low-temperature gas sensing properties. *Journal of Alloys and Compounds* [online]. 2019, **773**, 802–811. ISSN 09258388.

[29] HJIRI, M., EL MIR, L., LEONARDI, S.G., PISTONE, A., MAVILIA, L. and NERI, G. Al-doped ZnO for highly sensitive CO gas sensors. *Sensors and Actuators, B: Chemical* [online]. 2014, **196**, 413–420. ISSN 09254005.

[30] SONG, J., LIU, S., YANG, C., WANG, G., TIAN, H., ZHAO, Z. jian, MU, R. and GONG, J. The role of Al doping in Pd/ZnO catalyst for CO2 hydrogenation to methanol. *Applied Catalysis B: Environmental* [online]. 2020, **263**(November 2019), 118367. ISSN 09263373.

[31] JIANG, X., SONG, Z., LIU, G., MA, Y., WANG, A., GUO, Y. and DU, Z. AgNWs/AZO composite electrode for transparent inverted ZnCdSeS/ZnS quantum dot light-emitting diodes. *Nanotechnology* [online]. 2020, **31**(5). ISSN 13616528.

[32] GEDYE, R., SMITH, F., WESTAWAY, K., ALI, H., BALDISERA, L., LABERGE, L. and ROUSELL, J. The use of microwave ovens for rapid organic synthesis. *Tetrahedron Letters* [online]. 1986, **27**(3), 279–282. ISSN 00404039.

[33] ZHU, Y.J. and CHEN, F. Microwave-assisted preparation of inorganic nanostructures in liquid phase. *Chemical Reviews* [online]. 2014, **114**(12), 6462–6555. ISSN 15206890.

[34] HOWE, A.G.R., MIEDZIAK, P.J., MORGAN, D.J., HE, Q., STRASSER, P. and EDWARDS, J.K. One pot microwave synthesis of highly stable AuPd@Pd supported core-shell nanoparticles. *Faraday Discussions* [online]. 2018, **208**, 409–425. ISSN 13645498.

[35] SCHÜTZ, M.B., XIAO, L., LEHNEN, T., FISCHER, T. and MATHUR, S. Microwave-assisted synthesis of nanocrystalline binary and ternary metal oxides. *International Materials Reviews* [online]. 2017, **6608**(December), 1–34. ISSN 0950-6608.

[36] BILECKA, I. and NIEDERBERGER, M. Microwave chemistry for inorganic nanomaterials synthesis. *Nanoscale* [online]. 2010, **2**(8), 1358. ISSN 2040-3364.

[37] KOZAKOVA, Z., KURITKA, I., KAZANTSEVA, N.E., BABAYAN, V., PASTOREK, M., MACHOVSKY, M., BAZANT, P. and SAHA, P. The formation mechanism of iron oxide nanoparticles within the microwave-assisted solvothermal synthesis and its correlation with the structural and magnetic properties. *Dalton Transactions* [online]. 2015, **44**(48), 21099–21108. ISSN 14779234.

[38] SERNELIUS, B.E., BERGGREN, K.F., JIN, Z.C., HAMBERG, I. and GRANQVIST, C.G. Band-gap tailoring of ZnO by means of heavy Al doping. *Physical Review B* [online]. 1988, **37**(17), 10244–10248. ISSN 01631829.

[39] DJERDJ, I., ARČON, D., JAGLIČIĆ, Z. and NIEDERBERGER, M. Nonaqueous synthesis of metal oxide nanoparticles: Short review and doped titanium dioxide as case study for the preparation of transition metal-doped oxide nanoparticles. *Journal of Solid State Chemistry* [online]. 2008, **181**(7), 1571–1581. ISSN 00224596.

[40] MANZHI, P., KUMARI, R., ALAM, M.B., UMAPATHY, G.R., KRISHNA, R., OJHA, S., SRIVASTAVA, R. and SINHA, O.P. Mg-doped ZnO nanostructures for efficient Organic Light Emitting Diode. *Vacuum* [online]. 2019, **166**(November 2018), 370–376. ISSN 0042207X.

[41] BO, R., ZHANG, F., BU, S., NASIRI, N., DI BERNARDO, I., TRAN-PHU, T., SHRESTHA, A., CHEN, H., TAHERI, M., QI, S., ZHANG, Y., MULMUDI, H.K., LIPTON-DUFFIN, J., GASPERA, E. Della and TRICOLI, A. One-Step Synthesis of Porous Transparent Conductive Oxides by Hierarchical Self-Assembly of Aluminum-Doped ZnO Nanoparticles. *ACS Applied Materials and Interfaces* [online]. 2020, **12**(8),

9589–9599. ISSN 19448252.

[42] BUONSANTI, R. and MILLIRON, D.J. Chemistry of doped colloidal nanocrystals. *Chemistry of Materials* [online]. 2013, **25**(8), 1305–1317. ISSN 08974756.

[43] CHEN, W. *Doped nanomaterials and nanodevices. Vol. 1, Vol. 1,.* Stevenson Ranch: American Scientific Publishers, 2010. ISBN 1588831108 9781588831101 1588831078 9781588831071.

[44] PHAN, C.M. and NGUYEN, H.M. Role of Capping Agent in Wet Synthesis of Nanoparticles. *Journal of Physical Chemistry A* [online]. 2017, **121**(17), 3213–3219. ISSN 15205215.

[45] LI, C.C., CHANG, S.J., SU, F.J., LIN, S.W. and CHOU, Y.C. Effects of capping agents on the dispersion of silver nanoparticles. *Colloids and Surfaces A: Physicochemical and Engineering Aspects* [online]. 2013, **419**, 209–215. ISSN 18734359.

[46] DLAMINI, N.N., RAJASEKHAR PULLABHOTLA, V.S.R. and REVAPRASADU, N. Synthesis of triethanolamine (TEA) capped CdSe nanoparticles. *Materials Letters* [online]. 2011, **65**(9), 1283–1286. ISSN 0167577X.

[47] BHAWAWET, N., ESSNER, J.B., ATWOOD, J.L. and BAKER, G.A. On the non-innocence of the imidazolium cation in a rapid microwave synthesis of oleylamine-capped gold nanoparticles in an ionic liquid. *Chemical Communications* [online]. 2018, **54**(54), 7523–7526. ISSN 1364548X.

[48] SKODA, D., URBANEK, P., SEVCIK, J., MUNSTER, L., NADAZDY, V., CULLEN, D.A., BAZANT, P., ANTOS, J. and KURITKA, I. Colloidal cobalt-doped ZnO nanoparticles by microwave-assisted synthesis and their utilization in thin composite layers with MEH-PPV as an electroluminescent material for polymer light emitting diodes. *Organic Electronics* [online]. 2018, **59**(March), 337–348. ISSN 15661199.

[49] CUN, Y., SONG, C., ZHENG, H., WANG, J., MAI, C., LIU, Y., LI, J., YU, D., WANG, J., YING, L., PENG, J. and CAO, Y. Modifying the organic/metal interface *via* solvent vapor annealing to enhance the performance of blue OLEDs. *Journal of Materials Chemistry C* [online]. 2019. ISSN 2050-7526.

[50] CHOI, Y.J., PARK, H.H., GOLLEDGE, S. and JOHNSON, D.C. A study on the incorporation of ZnO nanoparticles into MEH-PPV based organic-inorganic hybrid solar cells. *Ceramics International* [online]. 2012, **38**(SUPPL. 1), S525–S528. ISSN 02728842.

[51] FRIEND, R.H., GYMER, R.W., HOLMES, A.B., BURROUGHES, J.H., MARKS, R.N., TALIANI, C., BRADLEY, D.D.C., SANTOS, D.A. Dos, BREDAS, J.L., LOGDLUND, M. and SALANECK, W.R. Electroluminescence in conjugated polymers. *Nature* [online]. 1999, **397**(6715), 121–128. ISSN 00280836.

[52] HUANG, J., XU, Z., ZHAO, S., LI, Y., ZHANG, F., SONG, L., WANG,

Y. and XU, X. Organic/inorganic heterostructures for enhanced electroluminescence. *Solid State Communications* [online]. 2007, **142**(7), 417–420. ISSN 00381098.

[53] LUKA, G., NITTLER, L., LUSAKOWSKA, E. and SMERTENKO, P. Electrical properties of zinc oxide – Tetracene heterostructures with different n-type ZnO films. *Organic Electronics: physics, materials, applications* [online]. 2017, **45**, 240–246. ISSN 15661199.

[54] NIKHIL, PANDEY, R.K., SAHU, P.K., SINGH, M.K. and PRAKASH, R. Fast grown self-assembled polythiophene/graphene oxide nanocomposite thin films at air-liquid interface with high mobility used in polymer thin film transistors. *Journal of Materials Chemistry C* [online]. 2018, **6**(37), 9981–9989. ISSN 20507526.

[55] PETRELLA, A., CURRI, M.L., STRICCOLI, M., AGOSTIANO, A. and COSMA, P. Photoelectrochemical properties of ZnO nanocrystals/MEH-PPV composite: The effects of nanocrystals synthetic route, film deposition and electrolyte composition. *Thin Solid Films* [online]. 2015, **595**, 157–163. ISSN 00406090.

[56] CHOI, Y.-J., GONG, S.C., PARK, C.-S., LEE, H.-S., JANG, J.G., CHANG, H.J., YEOM, G.Y. and PARK, H.-H. Improved performance of organic light-emitting diodes fabricated on Al-doped ZnO anodes incorporating a homogeneous Al-doped ZnO buffer layer grown by atomic layer deposition. *ACS Applied Materials and Interfaces* [online]. 2013, **5**, 3650–3655. ISSN 1944-8252.

[57] ZHANG, Y., SHAH, T., DEEPAK, F.L. and KORGEL, B.A. Surface Science and Colloidal Stability of Double-Perovskite Cs2AgBiBr6 Nanocrystals and Their Superlattices. *Chemistry of Materials* [online]. 2019, **31**(19), 7962–7969. ISSN 15205002.

[58] GYERGYEK, S., MAKOVEC, D. and DROFENIK, M. Colloidal stability of oleic- and ricinoleic-acid-coated magnetic nanoparticles in organic solvents. *Journal of Colloid and Interface Science* [online]. 2011, **354**(2), 498–505. ISSN 00219797.

[59] MANZHI, P., ALAM, M.B., KUMARI, R., KRISHNA, R., SINGH, R.K., SRIVASTAVA, R. and SINHA, O.P. Li-doped ZnO nanostructures for the organic light emitting diode application. *Vacuum* [online]. 2017, **146**, 462–467. ISSN 0042207X.

[60] CHEN, G., LIU, F., LING, Z., ZHANG, P., WEI, B. and ZHU, W. Efficient organic light emitting diodes using solution-processed alkali metal carbonate doped ZnO as electron injection layer. *Frontiers in Chemistry* [online]. 2019, **7**(MAR), 1–9. ISSN 22962646.

[61] JAMATIA, T., SKODA, D., URBANEK, P., SEVCIK, J., MASLIK, J., MUNSTER, L., KALINA, L. and KURITKA, I. Microwave-assisted synthesis of FexZn1−xO nanoparticles for use in MEH-PPV nanocomposites and their application in polymer light-emitting diodes.

Journal of Materials Science: Materials in Electronics [online]. 2019. ISSN 0957-4522.

[62] JAMATIA, T., SKODA, D., URBANEK, P., MUNSTER, L., SEVCIK, J. and KURITKA, I. Microwave-assisted particle size-controlled synthesis of ZnO nanoparticles and its application in fabrication of PLED device. *Journal of Physics: Conference Series* [online]. 2019, **1310**(1). ISSN 17426596.

[63] CICILIATI, M.A., SILVA, M.F., FERNANDES, D.M., DE MELO, M.A.C., HECHENLEITNER, A.A.W. and PINEDA, E.A.G. Fe-doped ZnO nanoparticles: Synthesis by a modified sol-gel method and characterization. *Materials Letters* [online]. 2015, **159**, 84–86. ISSN 18734979.

[64] KAYANI, Z.N., ABBAS, E., SADDIQE, Z., RIAZ, S. and NASEEM, S. Photocatalytic, antibacterial, optical and magnetic properties of Fe-doped ZnO nano-particles prepared by sol-gel. *Materials Science in Semiconductor Processing* [online]. 2018, **88**(May), 109–119. ISSN 13698001.

[65] RAJA, K., RAMESH, P.S. and GEETHA, D. Spectrochimica Acta Part A : Molecular and Biomolecular Spectroscopy Structural , FTIR and photoluminescence studies of Fe doped ZnO nanopowder by co-precipitation method. *Spectrochimica Acta Part a: Molecular and Biomolecular Spectroscopy* [online]. 2014, **131**, 183–188. ISSN 1386-1425.

[66] KARAMAT, S., RAWAT, R.S., LEE, P., TAN, T.L. and RAMANUJAN, R. V. Structural, elemental, optical and magnetic study of Fe doped ZnO and impurity phase formation. *Progress in Natural Science: Materials International* [online]. 2014, **24**(2), 142–149. ISSN 10020071.

[67] SEVCIK, J., URBANEK, P., DAVID, S., JAMATIA, T., NADAZDY, V., URBANEK, M., ANTOS, J., MUNSTER, L. and KURITKA, I. Role of aluminum-doped ZnO nanoparticles in thin nanocomposite active layer in fabrication of green/yellow and orange polymer LED. *To be submitted.* 2020.

[68] ŠEVČÍK, J. *Preparation and characterisation of nanocomposite thin films applicable in organic electronics* [online]. B.m., 2019. Tomas Bata University in Zlin.

[69] FIEVET, F., LAGIER, J.P. and FIGLARZ, M. Preparing Monodisperse Metal Powders in Micrometer and Submicrometer Sizes by the Polyol Process. *MRS Bulletin* [online]. 1989, **14**(12), 29–34. ISSN 19381425.

LIST OF TABLES

LIST OF FIGURES

LIST OF ABBREVIATIONS

CVD	Chemical vapour deposition
DEG	Diethylene glycol
DRUV-Vis	Diffuse reflectance ultraviolet visible spectroscopy
EDS	Electron dispersive spectroscopy
EL	Electroluminescence spectroscopy
FT-IR	Fourier-transform infrared spectroscopy
HDA	Hexadecylamine
HOMO	Highest occupied molecular orbital
ITO	Indium tin oxide
LUMO	Lowest unoccupied molecular orbital
MEH-PPV	Poly[2-methoxy-5-(2-ethylhexyloxy)-1,4-phenylene vinylene]
NBE	Near-band-edge
OA	Oleic acid
OLED	Organic light-emitting diode
OPV	Organic photovoltaic cell
PEDOT:PSS	poly(3,4-ethylenedioxythiophene) polystyrene sulfonate
PdI	Polydispersity index
PLED	Polymer light-emitting diode
PL	Photoluminescence
SEM	Scanning electron microscope
TEA	Triethylamine
TEM	Transmission electron microscope
TGA	Thermogravimetric analysis
TOPO	Trioctylphosphine oxide
UV-Vis	Ultraviolet visible spectroscopy
XPS	X-ray photoelectron spectroscopy
XRD	X-ray diffraction

LIST OF SYMBOLS

A	Absorbance	m_e^*	effective mass of excited electron
Acac	Acetylacetonate	m_h^*	effective mass of excited hole
Å	Angstrom	η	Dynamic viscosity
β	Full-width half maximum	n_{Zn}	Molar concentration of zinc
c	Molar concentration	n_{Fe}	Molar concentration of iron
d	Crystallite size	n_{Al}	Molar concentration of aluminium
d	Spacing between diffracting planes	OAc	Acetate
ε	Molar absorption coefficient	O_i	Oxygen interstitial
ε'	Dielectric constant	O_{Zn}	Oxygen substitute in zinc site
ε''	Dielectric loss	R	Absolute reflectance
eV	Electron volt	r	radius of the semiconductor
E	Energy of the incident photon	$\tan \theta$	Loss tangent
$E_{g(bulk)}$	band gap energy of the bulk semiconductor	T	Absolute temperature
$E_{g(nano)}$	band gap of a semiconductor nanoparticle	V_O	Oxygen vacancies
$E_{g(tr)}$	energy needed to create the lowest exciton energy	V_{Zn}	Zinc vacancies
$F(R)$	Kubelka-Munk function	ν	Frequency of the incident photon
h	Planck's constant	Zn_i	Zinc interstitial
K	Grain shape dependent	Zn_O	Zinc substitute in oxygen site
k	Boltzmann's constant	λ	Wavelength of the incident X-ray
M_w	Molecular weight	λ_{max}	Absorption peak maxima

CURRICULUM VITAE

Personal information

Name and surname   Thaiskang Jamatia

Nationality   Indian

Date of birth   6th October 1990

Address   nám. T. G. Masaryka 3050, 760 01 Zlín

Mobile number   +420 776643431

Email   jamatia@utb.cz

Education

2016-present   Tomas Bata University in Zlin,
                          PhD, Faculty of Technology,
                          Chemistry and Materials Technology,
                          Technology of Macromolecular Compounds

Internship   Freemovers Exchange Program
Sept. 2019- Dec. 2019   ETH Zurich, Rämistrasse 101,
                          8092 Zürich, Switzerland

2010-2015   Karunya University,
                          Integrated Masters in Science (MSc),
                          Nanoscience and Technology,
                          Coimbatore, India

2007-2010   Hindi Higher Secondary School
                          Agartala, India

List of projects

IGA/CPS/2017/008 — Preparation and characterization of nanoparticles and thin nanocomposite films made thereof – member of the research team- Project leader.

IGA/CPS/2018/007 — Development and studies of conductive nanocomposite systems applicable in polymer electronics – member of the research team- Member of research team.

IGA/CPS/2019/007 — Development and study of conductive nanocomposite materials for electronic and electrotechnical applications –Member of research team.

GA19-23647S (2019-2021) — Investigation of Correlation Among cation distribution, particle size and physical properties of intelligent spinel ferrite nanomaterials- Member of research team.

LIST OF PUBLICATIONS

Journal articles

1. Jamatia, T; Skoda, D; Urbanek, P; Sevcik, J; Maslik, J; Munster, L; Kalina, L; Kuritka, I. *Microwave-assisted synthesis of $Fe_xZn_{1-x}O$ nanoparticles for use in MEH-PPV nanocomposites and their application in polymer light-emitting diodes*. Journal of Materials Science: Materials in Electronics (2019) 30:11269–11281. DOI: https://doi.org/10.1007/s10854-019-01473-z.

2. Yadav, R. S.; Kuritka, I; Vilcakova, J; Jamatia, T; Machovsky, M; Skoda, D; Urbanek, P; Masar, M; Urbánek, M; Kalina, L; Havlica, J. *Impact of sonochemical synthesis condition on the structural and physical properties of $MnFe_2O_4$ spinel ferrite nanoparticles*. Ultrasonics Chemistry-Volume 61, March 2020, 104839. DOI: https://doi.org/10.1016/j.ultsonch.2019.104839.

3. Sevcik, J; Urbanek, P; Skoda, D; Jamatia, T; Nadazdy, V; Urbanek, M; Antos, J; Munster, L; Kuritka, I. Role of aluminum-doped ZnO nanoparticles in thin nanocomposite active layer in fabrication of green/yellow and orange polymer LED. To be submitted. 2020.

International conference proceedings (active presentation)

1. Jamatia, T; Skoda, D; Urbanek, P;Munster, L; Sevcik, J; Kuritka, I. *Tailoring of band gap and optical properties of ZnO nanoparticles by doping with Fe*. In: 22nd International Conference and Expo on Nanoscience and Molecular Nanotechnology, Frankfurt, Germany. DOI: 10.4172/2157-7439-C1-059.

2. Jamatia, T;   Skoda, D; Urbanek, P;Munster, L; Sevcik, J; Kuritka, I. *Microwave-assisted particle size-controlled synthesis of ZnO nanocolloids and its application in fabrication of PLED devices*: Applied Nanotechnology and Nanoscience International Conference, Berlin, Germany 2018, Journal of Physics: Conference series. DOI: 10.1088/1742-6596/1310/1/012012

Other conference contributions

3. Ševčík J; Škoda D.; Jamatia T.; Antoš J.; Urbánek P.; Kuřitka I. *Bandgap engineering of ZnO nanoparticles for polymer active layers in leds*: Plastko: sborník příspěvků z konference, 18. - 19. dubna 2018.

4. Ševčík J; Škoda D.; Jamatia T.; Antoš J.; Urbánek P.; Kuřitka I. *ZnO Particle Bandgap Engineering for Polymer Nanocomposites as Active Layers in LEDs:* Polymers : site of advanced horizons and ambits : May 2-4, 2018 Zlín, Czech Republic : P-SAHA 18 UTB.

5. Yadav R. S.; Kuřitka I.; Vilčáková J.; Škoda D.; Urbánek P.; Machovský M.; Jamatia T.; Masař M. *Particle Size, Cation Distribution and Magnetic Properties of Intelligent Spinel Ferrite Nanoparticles and its Application:* 2nd Global Conference on Magnetism and Magnetic Materials (GCMMM-2019), 25-26 July, Rome, Italy.

Thaiskang Jamatia

Preparation and characterisation of fillers for polymer nanocomposite layers usable in electronics

Příprava a charakterizace plniv pro polymerní nanokompozitní vrstvy využitelné v elektronice

Doctoral Thesis Summary